Spatially Resolved Transcriptomic Signatures of Hippocampal Subregions and *Arc*-Expressing Ensembles in Active Place Avoidance Memory

Authors: Isaac Vingan[1], Victoria Sook Keng Tung[2], Shwetha Phatarpekar[3], A. Iván Hernández[1,4,6], Oleg V. Evgrafov[2,3,5], Juan Marcos Alarcon[1,4,6,#]

Affiliations:

[1]School of Graduates Studies, Program in Neural and Behavioral Sciences, State University of New York, Downstate Health Sciences University, Brooklyn, NY, USA

[2]School of Graduates Studies, Program in Molecular and Cell Biology, State University of New York, Downstate Health Sciences University, Brooklyn, NY, USA

[3]Institute of Genomic Health, State University of New York, Downstate Health Sciences University, Brooklyn, NY, USA

[4]Department of Pathology, State University of New York, Downstate Health Sciences University, Brooklyn, NY, USA

[5]Department of Cell Biology, State University of New York, Downstate Health Sciences University, Brooklyn, NY, USA

[6]The Robert F. Furchgott Center for Neural & Behavioral Science, State University of New York, Downstate Health Sciences University, Brooklyn, NY, USA

#Corresponding author: Juan Marcos Alarcon (juanmarcos.alarcon@downstate.edu)

KEYWORDS

Spatial Transcriptomics, Gene Expression, Memory, Hippocampus, CA1, CA3, Dentate Gyrus, Immediate Early Gene, IEG-Expressing Ensemble, Memory-associated Neuronal Ensemble

ACKNOWLEDGEMENTS

Supported by Senior Vice President of Research Seed Grant (State University of New York, Downstate Health Sciences University) and partial support from NINDS grant R21NS091830.

FINANCIAL DISCLOSURES

The authors declare there are no competing financial or non-financial interests.

Year: 2023

ABSTRACT

The rodent hippocampus is a spatially organized neuronal network that supports the formation of spatial and episodic memories. We conducted bulk RNA sequencing and spatial transcriptomics experiments to measure gene expression changes in the dorsal hippocampus following recall of active place avoidance memory. Our analysis focused on two specific levels of spatial resolution: hippocampal subregions and Immediate Early Gene (IEG) expressing cellular assemblies. Through bulk RNA sequencing, we examined the gene expression changes following memory recall across the functionally distinct subregions of the dorsal hippocampus. We found that training induced differentially expressed genes (DEGs) in the CA1 and CA3 hippocampal subregions were enriched with genes involved in synaptic transmission and synaptic plasticity, while DEGs in the dentate gyrus (DG) were enriched with genes involved in energy balance and ribosomal function. Through spatial transcriptomics, we examined gene expression changes following memory recall in putative memory-associated neuronal ensembles marked by the expression of the IEGs *Arc*, *Egr1*, and *c-Jun*. Within samples from both trained and untrained mice, the subpopulations of spatial transcriptomic spots marked by these IEGs were functionally and spatially distinct from one another. In only the hippocampus of trained mice, DEGs detected between Arc+ and Arc- spots were enriched in several memory-related gene ontology terms, including "regulation of synaptic plasticity" and "memory." Our results suggest that memory recall is supported by region-specific gene expression changes and transcriptionally distinct IEG expressing ensembles of neurons in the hippocampus.

57 **INTRODUCTION**

58 The neural operations supporting memory require the involvement of various brain systems
59 interconnected through neural networks [1]. The activity of these networks is fine-tuned by
60 experience through the selective recruitment of ensembles of neurons ascribed to contain the bits
61 of information associated with memory [2]. Neuronal ensemble activity is shaped by synaptic
62 plasticity mechanisms that modulate the weight and efficacy of the ensemble's synaptic
63 connections [3, 4]. Changes in gene expression are a key underlying mechanism in synaptic
64 plasticity [5], and recent studies have identified multiple profiles of gene expression associated
65 with memory [6-8].

66 In the rodent hippocampus, encoding of spatial memory information is supported by the diversity
67 of synaptic computations within and across its sub-fields [9, 10]. Each hippocampal subregion
68 (i.e. Dentate Gyrus, CA1, CA2, CA3) shows distinct patterns of activity to process spatial
69 information and to form or retrieve memories [11-16]. At the regional level, patterns of activity
70 are conferred through the combination of cyto-architecture, local synaptic circuitry, neuronal
71 cell types and synaptic inputs unique to each region [7, 13, 17-26]. At the single-cell level, the
72 functional state of hippocampal neurons is defined by connectivity, hippocampal subregional
73 location, and experience-dependent recruitment into a memory ensemble [2, 27].

74 The investigation of memory across molecular and functional levels necessitates an approach
75 that connects the scales of hippocampal organization between cellular mechanisms and networks
76 of cells. While the functional contribution of individual genes that underly synaptic plasticity at
77 the cellular level are well-established [4, 28-31], it remains unclear what changes in gene
78 expression across hippocampal subregions and subpopulations of the memory-associated
79 neuronal ensembles characterize memory in the hippocampus.

80 Memory-associated neuronal ensembles are a sparsely distributed population of neurons that
81 strongly activate together during the acquisition and recall of a memory, and are thought to
82 encode the particular bits of information relevant to that memory [20, 32, 33]. Numerous studies
83 have identified Immediate Early Genes (IEGs) such as *Arc*, *c-Fos*, *Egr1*, *c-Jun*, *Npas4*, *Bdnf*, and
84 *Fmrp* to characterize memory-associated neuronal ensembles [2, 34-36]. In this study, the
85 location of memory-associated neuronal ensembles is inferred from the expression of IEGs in
86 spatial transcriptomic spots. The expression of *Arc* mRNA has been used to tag and characterize
87 the properties of memory-associated neuronal ensembles [37-39]. This proxy for the memory-
88 associated neuronal ensemble was used to explore the transcriptomic changes supporting
89 memory recall in the hippocampus. We characterized changes in gene expression across the
90 major subregions of the transverse dorsal hippocampus using bulk RNA sequencing of micro-
91 dissected dorsal hippocampal subregions, and investigated the spatial distribution of IEG-
92 associated gene expression through a spatial transcriptomic study of coronal dorsal hippocampal
93 slices.

RESULTS

APA trained mice exhibit place avoidance memory

To investigate gene expression changes induced by active place avoidance (APA) training in the hippocampal network, we conducted bulk RNA-sequencing and spatial transcriptomics (see Figure 1A for experimental timeline). In the APA, mice learn to avoid a 60° shock zone on a rotating circular arena [40, 41]. Mice trained in the APA showed a decrease in the number of shocks delivered during the acquisition trials (Figure 1B) and longer re-entry times to the shock zone during the memory retention test trials (Figure 1C).

Bulk RNA-seq transcriptomic profiling DG, CA3 and CA1 separate trained from untrained cohorts

To explore the molecular mechanisms underlying memory recall across the dorsal hippocampus, bulk RNA-sequencing was performed on microdissected DG, CA3 and CA1 hippocampal subregions. Principal component analysis (PCA) from all 3 subregions combined reveals a separation of samples by behavioral cohort (Figure 2A), indicating that differences in training contributes substantially to the overall variability of gene expression in our samples. Separation between samples is further accentuated when PCA is performed separately on data from each subregion (Figure 2C-D). Consistently, hierarchical clustering of gene expression profiles reliably grouped samples by their behavioral cohort (Figure 2E).

Synaptic plasticity and learning and memory-related biological processes are regionally enriched

We detected 1663, 606, 315 and 350 differentially expressed genes (DEGs) (adjusted p-value < 0.05) between trained and untrained samples for the combined hippocampal subregions and

118 separated CA1, CA3, and DG subregions, respectively (Figure 3A-D). 966 genes were
119 upregulated and 697 were downregulated in all hippocampal subregions. In CA1 393 genes were
120 upregulated and 213 were downregulated, in CA3 273 genes were upregulated and 42 were
121 downregulated, and in DG 117 genes were upregulated and 223 were downregulated.
122 In each comparison the majority of highly significant DEGs (FDR < 0.005) exhibited a modest
123 effect size ($|\log_2 \text{fold}| < 1.0$). Among these DEGs in the combined subregions with a high
124 significance and modest effect size, there are the genes *Ywhag*, *Bsn*, and *Nup153*, which are
125 related to cell signaling and morphogenesis [42-44]. In the CA1, we found *Camk2n1*, *Shank3*,
126 *Shank1*, and *Snap* 25 which are related to synaptic signaling and plasticity [45-48]. We found
127 *Prckg*, Ttr, and *Snhg11* in the CA3 which are related to memory [49-51]. *Kit*, *Srrm1*, and *Syn2*,
128 found in the DG, are related to cell morphogenesis and synaptic signaling [52-54].
129 To further elucidate the distribution of DEGs across hippocampal subregions we investigated the
130 overlap of significant DEGs (FDR < 0.05). We found the largest overlap of upregulated DEGs
131 between the CA3 and CA1 subregions with a total of 127 intersecting genes (Figure 3E). The
132 genes *Snap25, Shank1, Shank 3, Bsn and Ywhag* were identified in the overlap between the
133 upregulated DEGs of CA3 and CA1 and are known for their involvement in synaptic plasticity.
134 *Ywhag* was also found to be upregulated in the overlap of all three subregions.
135 Next, we performed Gene Ontology (GO) enrichment analyses to annotate each subregion (i.e.,
136 DG, CA3 and CA1) with GO terms overrepresented amongst the DEGs detected in each
137 subregional analysis [55]. In all hippocampal regions combined, we found DEGs were
138 significantly enriched with genes involved in synaptic machinery (Figure 3F & Supplemental
139 Figure 1F,G). Upregulated DEGs detected in both the CA3 and CA1 were enriched with genes
140 involved in synaptic transmission. Upregulated DEGs detected in the DG were enriched with

141 genes involved in neurogenesis and ATP production. In the DG downregulated DEGs were
142 involved in transcriptional machinery and epigenetic modifications (Figure 3F). Downregulated
143 DEGs in the CA1 and CA3 were not significantly enriched with any biological processes. These
144 data reveal a spatial distribution of gene expression across the dorsal hippocampus, defined by a
145 greater degree of similarity between the CA1 and CA3 than between either of these subregions
146 and the DG.
147
148 **Differences in the spatial distribution of hippocampal gene expression between trained and**
149 **untrained animals**
150 To further investigate the spatial distribution of DEGs associated with APA memory across the
151 hippocampus, we performed spatial transcriptomics on coronal sections containing the dorsal
152 hippocampus from one trained and one untrained mouse. Computational analyses of integrated
153 capture spots in the hippocampus of trained and untrained samples reveals distinct clusters (seen
154 in a Uniform Manifold Approximation and Projection (UMAP) plot) which map along
155 anatomical boundaries in a spatial transcriptomic plot (Figure 4A,B). Spatial transcriptomic data
156 were integrated with the Allen Brain Atlas to computationally annotate each spot with the cell-
157 type most prominently detected [56] (Figure 4C,D).
158 We detected 352 DEGs in all hippocampal spots (205 upregulated and 147 downregulated genes)
159 between trained and untrained samples. 75 DEGs in the CA1 cell layer (55 upregulated and 20
160 downregulated genes), 72 DEGs in the CA3 cell layer (54 upregulated and 18 downregulated
161 genes), and 187 DEGs in the DG cell layer (129 upregulated and 58 downregulated genes)
162 (Figure 5 A-D). Genes *Cnih2, Syn1,* and *Camk2b,* were differentially expressed in the CA1,

163 CA3, and DG, respectively. These genes are involved in synaptic plasticity and learning and
164 memory [57-59].
165 In the comparison of DEGs between all hippocampal spots, GO enrichment analyses identified
166 biological processes related to synaptic plasticity and synaptic signaling (Figure 5F &
167 Supplemental Figure 2B,C). In the CA1 and CA3 subregions, we found upregulation of genes
168 involved in biological processes also related to synaptic plasticity and synaptic signaling (Figure
169 5F). In the DG upregulated DEGs were enriched in biological processes involved in protein
170 expression and ribosomal function (Figure 5F). CA1 was the only subregion where
171 downregulated DEGs show enrichment for biological processes. Our results show a high
172 similarity in the biological functions overrepresented in both the spatial transcriptomic and bulk
173 RNA sequencing differential gene expression analyses between trained and untrained samples.
174

175 **Arc-expressing hippocampal spots exhibit changes in the expression of memory-associated**
176 **genes and biological processes**

177 Our data suggest that differences in behavioral conditioning contributed to variations in the
178 spatial distribution of synaptic plasticity related gene expression across the hippocampal
179 network. Differences in behavioral conditioning affect the recruitment of Arc-expressing
180 hippocampal neurons which form the memory-associated neuronal ensemble [60-63]. We
181 studied the *Arc*-expressing spatial transcriptomics spots as a proxy for the putative IEG tagged
182 memory-associated neuronal ensemble to assess changes in biological processes following APA
183 memory recall. Out of the 542 spots in the hippocampus from the trained sample, 195 spots had
184 detectable expression of *Arc* mRNA (*Arc*+). In the untrained sample, 169 out of 568

185 hippocampal spots were *Arc*+ (Supplemental Figure 3G). In both samples, spots with the highest
186 level of *Arc* expression were located in the CA1 cell layer (Figure 6A,B).
187 To test whether *Arc*-expressing neuronal ensembles exhibit changes in the expression of genes
188 related to synaptic plasticity, we performed differential gene expression analyses between both:
189 *Arc*+ spots across trained and untrained samples (TR^{Arc+} vs. UT^{Arc+}), and between *Arc*+ and *Arc*-
190 spots within each sample (TR^{Arc+} vs. TR^{Arc-} & UT^{Arc+} vs. UT^{Arc-}) (Figure 6 C-F). Comparison of
191 TR^{Arc+} vs. UT^{Arc+} spots detected 174 significant DEGs (85 upregulated and 89 downregulated
192 genes), and comparison of TR^{Arc-} vs. UT^{Arc-} detected 353 significant DEGs (113 upregulated and
193 240 downregulated genes) (Figure 6 C,D). *Bc1* and *Rac1*, known for their involvement in
194 learning and memory [64, 65], were found to be down- and upregulated, respectively, in the
195 analysis across both *Arc*+ and *Arc*- spots. GO term enrichment analysis of upregulated DEGs
196 detected across the TR^{Arc+} vs. UT^{Arc+} showed enrichment with biological processes related to
197 synaptic signaling and protein translation (Figure 6 H & Supplemental Figure 3C,E).
198 Upregulated DEGs detected across the TR^{Arc-} vs. UT^{Arc-} spots enriched for genes related to
199 synaptic transport and plasticity. Conversely, across both TR^{Arc+} vs. UT^{Arc+} and TR^{Arc-} vs. UT^{Arc-}
200 spots, functions related to energy balance and protein translation were downregulated.
201 101 DEGs (95 upregulated, 6 downregulated) were detected within TR^{Arc+} vs. TR^{Arc-}, and 78
202 DEGs (47 upregulated, 31 downregulated) were detected within UT^{Arc+} vs. UT^{Arc-} (Figure 6 E,F).
203 *Dkk3*, *Cck*, and *Neurod6*, all genes related to learning and memory, were detected in *Arc*+ spots
204 within the hippocampus from both the trained and untrained mice [66-68]. *Homer1*, *Sv2b*, and
205 *Scn3b* were among the 17 significant DEGs detected in both the analysis of TR^{Arc+} vs. TR^{Arc-}
206 spots and the bulk comparison of all subregions. While DEGs detected within UT^{Arc+} vs. UT^{Arc-}
207 spots were not significantly enriched with genes involved in any biological processes, TR^{Arc+} vs.

208 TR^{Arc-} spots were significantly enriched with upregulated DEGs involved in synaptic plasticity
209 (Figure 6 G & Supplemental Figure 3D,F).
210
211 **IEG-expressing hippocampal spots comprise distinct gene expression profiles within**
212 **trained and untrained samples**
213 Subsets of the complete memory-associated neuronal ensemble can be marked through the
214 expression of different IEGs [69, 70]. To evaluate the functional relationship between these
215 subsets of the ensemble we correlated the expression of 22 known neuronal IEGs [71, 72] with
216 the expression of *Arc.* Pairwise correlations of the expression of these IEGs identified *Egr1* and
217 *c-Jun* as the IEGs most and least correlated with *Arc*, respectively (Supplemental Figure 3 A,B).
218 The correlation coefficients for *Arc* and *Egr1* are $r(21) = .598$, $p = 2.24 \times 10^{-56}$ in the untrained
219 sample and $r(21) = .764$, $p = 5.45 \times 10^{-105}$ in the trained sample. The correlation coefficients for
220 *Arc* and *c-Jun* are $r(21) = -.057$, $p = 0.17$ in the untrained sample and $r(21) = -.105$, $p = 0.014$ in
221 the trained sample. Because of this, we performed differential gene expression analyses on *Egr1*
222 and *c-Jun* expressing spots across and within behavioral conditions.
223 In total, 380 out of 542 spots in the hippocampus of the trained animal and 256 out of 568 in the
224 untrained were found to express detectable levels of *Egr1* (Supplemental Figure 3G). In both
225 samples, spots with the highest level of *Egr1* expression were located predominantly in the CA1
226 cell layer, following the spatial distribution of *Arc* expression. For the *Egr1*-expressing spots,
227 555 DEGs (509 upregulated, 46 downregulated) were identified the trained animal, and 196
228 DEGs (150 upregulated, 46 downregulated) in the untrained animals (Figure 7 D,F). In total, we
229 found detectable levels of *c-Jun* in 308 out of 542 spots in the hippocampal sample from the
230 trained animal and 175 out of 568 in the untrained animal (Supplemental Figure 3G). In both

231 samples, spots with the highest level of *c-Jun* expression were located predominantly in the DG
232 granule cell layer. For the *c-Jun*-expressing spots, 480 DEGs (440 upregulated, 40
233 downregulated) were identified within the trained animal, and 166 DEGs (138 upregulated, 28
234 downregulated) within the untrained animal (Figure 7 J,L).
235 Due to the high degree of correlation between the expression of *Arc* and *Egr1*, and the low
236 correlation between the expression of *Arc* and *c-Jun*, we predicted that *Arc* and *Egr1*-expressing
237 spots would appear more functionally similar to one another than they would to *c-Jun*-expressing
238 spots. However, GO enrichment analyses of all three IEG expressing spot populations across
239 trained and untrained conditions showed similar sets of enriched biological processes (Figure 7M
240 & Supplemental Figure 3C,E), namely those involved in gene expression and energy balance.
241 In contrast to the within sample analyses of *Arc*+ spots showing overrepresentation of biological
242 process only in the hippocampus of the trained mouse (Figure 6G), analyses of *Egr1*+ and *c-*
243 *Jun*+ spots in the hippocampal samples of *both* trained and untrained mice revealed DEGs that
244 were enriched in numerous biological processes. Biological processes enriched among DEGs in
245 the *Egr1*+ spots within the hippocampus of trained and untrained mice were similar, and
246 involved in synaptic plasticity and transmission (Figure 7N & Supplemental Figure 3C,E).
247 Additionally, in the hippocampus of the trained mouse, *Egr1*+ spots show downregulation of
248 biological processes related to protein translation and ribosomal function. A distinct collection of
249 biological processes were enriched among DEGs detected in analysis of *c-Jun*+ spots within the
250 trained and untrained samples. Biological processes involved in axonal growth and
251 neurotransmitter release were overrepresented in *c-Jun*+ spots in both the hippocampal sections
252 from trained and untrained mice.

253 **RT-qPCR of DEGs detected in the overlap between bulk RNA sequenced hippocampal**
254 **subregions**

255 To further validate the spatial distribution of DEGs across the hippocampal network, we
256 performed RT-qPCR comparisons of relative gene expression in micro-dissected DG, CA3, and
257 CA1 subregions (6 trained and 4 untrained animals). To support the regionalized differential
258 expression of the genes identified in the bulk RNA sequencing data, we measured the expression
259 of *Kit*, *Sst*, *Cdh24* (identified in the DG, CA3, CA1 subregions, respectively). *Gapdh* expression
260 was measured as an internal control. Expression of *Slc6a7* was also measured. *Slc6a7* was found
261 to be upregulated in all regional analyses (Figure 3E, center sector). Relative gene expression
262 demonstrate a significant upregulation of *Kit* in the DG of trained animals (p-adj = 0.024). *Sst*
263 was also found to be upregulated in the DG (Supplemental Figure 4A). We found no significant
264 differences for the measured genes in CA3 (Supplemental Figure 4B). In CA1, *Cdh24* is
265 increased in trained compared to untrained samples although the difference did not reach
266 statistical significance (Supplemental Figure 4C). And, *Slc6a7* was not increased in any
267 subregion.

268 **DISCUSSION**

269 In this study, we used a combination of bulk RNA sequencing and spatial transcriptomics to
270 identify changes in gene expression within major subregions of the dorsal hippocampus and
271 within IEG-expressing spots following APA memory recall. We hypothesized that forming a
272 memory-associated neuronal ensemble following memory training and recall leads to the
273 enrichment of unique biological processes across the dorsal hippocampus. To test this
274 hypothesis, we used a combination of bulk RNA sequencing and spatial transcriptomics to
275 identify changes in gene expression within each major subregion of the dorsal hippocampus and
276 within IEG-expressing spots following memory recall. Vanrobaeys et al. used spatial
277 transcriptomics to study consolidation of a spatial memory and found distinct yet overlapping
278 transcriptomic signatures across hippocampal subregions, with the CA1 and DG exhibiting
279 upregulation of genes related to transcriptional regulation and protein folding, respectively [73].
280 The findings from this study illustrate the importance exploring the spatial distribution of gene
281 expression profiles when investigating the memory-associated neuronal ensemble and the
282 functional changes therein.

283

284 **Regionalization of molecular mechanisms following memory recall**

285 Different brain regions are recruited depending on the type of memory training an animal is
286 exposed to [27, 74]. We found evidence supporting the regionalization of differential gene
287 expression and overrepresentation of GO terms (corresponding to specific biological processes)
288 across the dorsal hippocampus following spatial memory recall. Bulk RNA sequencing analyses
289 between trained and untrained samples revealed significant similarities in the DEGs detected in
290 CA1 and CA3 fields, but not between either of these subregions and the DG. Similarly, the

291 biological processes overrepresented amongst DEGs in the CA1 and CA3 subregions shared
292 more similarities than with those in the DG. Spatial transcriptomics also revealed regional
293 differences in DEG detection and biological process overrepresentation. DEGs detected via
294 spatial transcriptomics did not show considerable overlap compared with those detected via bulk
295 RNA sequencing. Such differences might be accounted for by the technical differences between
296 the two transcriptomic methodologies (addressed below).
297 Cells in the CA1 and CA3 subregions share similar morphologies and ontology as compared to
298 the dentate gyrus [75-77], which could account for our regionalized findings in the bulk RNA
299 sequencing study. During memory recall, the functional coupling of the CA3 and CA1
300 subregions [78, 79] is also reflected by the gene expression changes observed in this study. Our
301 data show that the spots in the CA3 and CA1 subregions have upregulated biological processes
302 involved in post synaptic machinery and synaptic plasticity, while the spots in the DG subregion
303 have upregulated processes involved in protein expression and energy balance, and have
304 downregulated processes involved in synaptic transmission. The cellular and molecular
305 modifications occurring during memory recall are known to include: 1) increases in neurogenesis
306 and protein synthesis in the DG [80-83] and 2) increased synaptic efficacy (e.g., LTP) across the
307 Schaffer collateral between the CA3 and CA1 [84, 85]. The overrepresentation of GO terms
308 involved in ATP metabolism and energy balance in the DG could indicate an understudied role
309 of the differential regulation of metabolic pathways in support of memory storage and recall in
310 the hippocampus [86, 87]
311 Circuitry in the hippocampus is differentially recruited depending on the phase, cognitive
312 demand, and valance of a memory[88-90]. We believe that the functional changes observed
313 during the recall phase of memory are one snapshot of the spatio-temporal modifications

occurring over the life of a memory in the brain. More studies are required to evaluate sequential changes in regionalized hippocampal function with memory over time.

Technical considerations of using spatial transcriptomics to study memory-associated neuronal ensembles

We utilized a combination of bulk RNA-seq and spatial transcriptomics to measure the gene expression changes in the brain following memory recall. Both methodologies provided unique utility and insight into the transcriptomic changes in the brain following memory and have proven to be highly compatible [73, 91]. We observed strong regionalized differences between training conditions, despite the fact that the changes we observed did not align between the two transcriptomic techniques. This discrepancy can be accounted for by some of the chemical and technical differences between the two methodologies. First, 10x's Visium spatial transcriptomic platform permits a granular resolution of neuronal systems with its 55µm diameter capture spots [92]. The resolution of this platform allows us to analyze gene expression differences between specifically annotated populations of neurons in the cell layers of each hippocampal subregion, rather than the entirety of the bulk section. Second, relative to bulk sequencing, 10x's Visium spatial transcriptomics requires more tissue processing before RNA extraction and has lower RNA detection sensitivity [93]. Consequently, some DEGs with lower levels of expression in our bulk study may have gone undetected in the spatial transcriptomic study, thus skewing which genes were profiled. Our study is amongst the first to examine gene expression changes within individual cell populations across a spatially distributed neuronal network. The exploratory nature of the present study, together with more accessible and higher resolution spatial

336 transcriptomic methods, is expected to develop into deeper characterizations of the mechanistic
337 architecture of memory.
338
339 ***Arc*-expressing spots are enriched with genes involved in synaptic plasticity**
340 Using spatial transcriptomics, we were able to detect the spatial distribution of immediate early
341 gene expression in the dorsal hippocampus. Spatial transcriptomic spots sample regions 55µm in
342 diameter, which can contain more than a dozen cell bodies (depending on the brain region). We
343 inferred that groups of IEG-expressing memory-associated neurons would be sampled by these
344 spots, which we predicted would be enriched with genes related to synaptic plasticity. To
345 accomplish this, we targeted the expression windows of both immediate early genes and late
346 response genes by sacrificing mice following the retention test during the peak of IEG expression
347 and the beginning of late response gene expression [94, 95].
348 Data from the *Arc*-expressing spots highlight the distinct gene expression profile of TR^{Arc+} spots.
349 Only the upregulated DEGs detected in the analysis of TR^{Arc+} vs. TR^{Arc-} were enriched with any
350 biological process. This pattern of enrichment indicates both that TR^{Arc+} neurons are functionally
351 distinct from the surrounding TR^{Arc-} cells and the UT^{Arc+} cells. Specifically, TR^{Arc+} cells are
352 defined by an upregulation and enrichment of biological processes related to synaptic plasticity,
353 a number of which were also upregulated and enriched in the bulk differential expression
354 analyses of all hippocampal regions combined. These data suggest that the functional changes
355 induced in the *Arc*-expressing spots might substantially contribute to the differences observed
356 between training conditions in the analysis of bulk hippocampal subregions. We also detected
357 DEGs and biological processes between the TR^{Arc+} vs. UT^{Arc+} spots. In addition to biological
358 processes related to synaptic signaling, an abundance of biological processes related to energy

359 metabolism and protein translation –ATP metabolic process, ATP synthesis coupled proton
360 transport and cytoplasmic translation – were enriched in the TR^{Arc+} vs. UT^{Arc+} comparison.
361 It is not yet known if the functional changes that distinguish cell in a memory-associated
362 neuronal ensemble from the surrounding cells are the same functional changes that distinguish
363 these cells across training conditions. Our data suggests that there are two defining features of
364 the *Arc*+ spots. The first is the upregulation of synaptic plasticity mechanisms when compared to
365 *Arc*- spots. This finding is supported by a recent study that found synaptic plasticity mechanisms
366 as a defining feature of a neuron in a memory-associated neuronal ensemble [96]. The second is
367 the increased recruitment of cellular machinery involved in energy production when compared to
368 the same spots in the hippocampus of the untrained animal. This result is supported by increases
369 in energy production and consumption during periods of high cognitive demand on neuronal
370 systems [97] In the case of the APA, the trained avoidance behavior is considered higher
371 cognitive demand than the untrained context habituation behavior [40, 98]. Arc+ spatial spots in
372 the trained animal are different from Arc- spots in the same animal and Arc+ spots in the
373 untrained animal.
374
375 ***Egr1*- and *c-Jun*-expressing spots exhibit distinct transcriptomic profiles**
376 The neuronal ensemble tagged by Arc is well studied for its role in memory storage and
377 maintenance [99], but the *Arc*-tagged ensemble encompasses only a subset of the neurons that
378 were active during a memory experience[69, 99, 100]. Subpopulations of this memory-associated
379 neuronal ensemble across brain systems might encode for multiple memory traces relevant to a
380 behavioral experience [1, 27, 101, 102]. Separate subpopulations of these neuronal ensembles are
381 tagged by at least one of the two dozen IEGs, the expression of which is linked to one of the

382 many patterns of strong neuronal activity elicited during a memory experience [27, 71, 103-105].
383 With spatial transcriptomics, we assessed gene expression profiles of IEG positive spots in the
384 dorsal hippocampus after the retention test in trained and untrained animals. We expanded our
385 investigation of the gene expression profile of the memory-associated neuronal ensemble to the
386 spots tagged by the IEGs *Egr1* and *c-Jun.* The expression of *Egr1* was most correlated with the
387 expression of *Arc,* while *c-Jun* was the least correlated.
388 Sparing some overlap, the populations of *Arc+, Egr1+,* and *c-Jun+* spots within both samples
389 were each enriched with genes involved in distinct collections of biological processes. DEGs
390 detected in the analysis of *Egr1+* and *c-Jun+* spots in *both* samples from trained and untrained
391 mice were enriched in numerous biological processes. However, DEGs detected in the analysis
392 of *Arc+* spots within *only* the trained sample were enriched with any biological processes,
393 namely those related to synaptic plasticity and synaptic function. The *Egr1+* spots within both
394 training conditions detected upregulated genes involved in biological processes related to
395 synaptic plasticity and synaptic transmission. *c-Jun+* spots within both training conditions
396 detected upregulated genes involved in biological processes related to axonal growth and
397 neurotransmitter release. Unlike the *Arc*-expressing spots in the trained sample, biological
398 process were enriched among downregulated DEGs detected *Egr1-* and *c-Jun*-expressing spots
399 the trained sample. Additionally, the spatial distribution of *Arc* and *Egr1* shows high levels of
400 expression in the CA1 cell-layer of trained and untrained samples, while the expression of *c-Jun*
401 is high in the DG. Expression of each IEG might be linked to particular patterns of neuronal
402 activation [106-108] [109] and output circuit function [89], highlighting the functional and
403 spatial diversity amongst recruited cells within memory associated neuronal ensembles. *Egr1* and
404 *c-Jun* expression are associated with fear memory and acute stress, respectively [110-112].

405 Perhaps, the differences observed amongst the *Egr1*+ and *c-Jun*+ spots may not be specific to
406 the behavior of trained active place avoidance behavior, but rather, sensitive to the shared
407 emotional, temporal and contextual components inherit to both long term memory experiences of
408 trained and untrained animals in the APA apparatus.
409 In contrast to the diversity of biological processes enriched among the DEGs between IEG-
410 expressing spots *within* each training condition, we found very similar collections of biological
411 processes in the GO enrichment analysis of IEG+ spots *across* training conditions. These
412 differentially regulated processes involved in energy production suggest that the training
413 experience induces a greater energy demand on the memory associated neuronal ensemble,
414 relative to the untrained experience. These data further highlight the need for greater energy
415 metabolism in higher cognitive demand memory experience, like that of training in the APA [87,
416 97].
417
418 **Investigating memory across multiple scales in the brain**
419 In summary, we performed an investigation of the transcriptomic profile of spatial memory recall
420 in the hippocampus using a combination of bulk RNA sequencing and spatial transcriptomics.
421 We found a regionalized pattern of gene expression with the CA1 and CA3 subregions being
422 enriched with genes involved in synaptic plasticity and transmission, while the DG subregion
423 was enriched with genes involved in protein expression and energy production. We also
424 discovered a unique transcriptomic profile of *Arc* expressing spots in the dorsal hippocampus of
425 trained mice enriched for upregulated genes involved synaptic plasticity and transmission.
426 Additionally, the transcriptomic profile of these *Arc* expression spots differed from those other
427 IEG expressing spots (i.e. *Egr1* and *c-Jun*).

428 This is amongst the first steps toward bridging our understanding of memory *across* scales
429 ranging from systems to cells to molecules. In this study, we investigate the spatial distribution
430 of memory-associated molecular function following the reactivation of a memory experience.
431 Through the joint investigation of the effectors of memory – their neuronal identities, spatial
432 location and functional changes – we open the opportunity for future studies that seek to
433 understand how memories are stored in the brain and how they change over time. Through
434 similar transcriptomic approaches that focus on space as a biologically relevant variable, we will
435 begin to map the distribution of memory-associated neuronal ensembles and their respective
436 gene expression changes as they undulate across the hippocampal network over the lifetime of
437 particular memory experiences.

METHODS

Animals

A total of 18 adult ArcCreERT2::eYFPflx mice [113] with C57BL/6 genetic background aged 3-4 months were used in this study (Bulk RNA sequencing – 3 male and 3 female, spatial transcriptomics – 2 male, RT-qPCR – 10 male). Mice were bred in-house at the SUNY Downstate Health Sciences University vivarium (Brooklyn, NY, USA). Mice were housed in groups of two to five until the start of the experiment, at which point they were single-housed in shoebox cages in a sound attenuation cubicle (Med Associates). For every experimental run, a minimum of two mice —each undergoing the same behavioral conditioning— were simultaneously housed in the sound attenuation cubicle. Ad libitum food and water was provided. Mice were randomly assigned to behavioral cohorts before the start of the experiment. Mice were handled daily for 3 days prior to the start of the experiment to reduce anxiety and improve voluntary approach. All animal procedures proposed are approved by, and will be performed following, the Institutional Animal Care and Use Committee guidelines at SUNY Downstate Health Sciences University.

Behavior

All procedures were performed in compliance with the Institutional Animal Care and Use Committee of the State University of New York, Downstate Health Sciences University. ArcCreERT2::eYFPflx male mice were trained in a hippocampus-dependent two-frame active place avoidance task. The place avoidance system consisted of a 40-cm diameter arena with a parallel rod floor that could rotate at 1 rpm. The position of the animal was tracked using PC-based software (Tracker, Bio-Signal Group Corp., Brooklyn, NY) that analyzed 30-Hz digital

461 video images from an overhead camera. Mice in the trained condition learned the
462 "Room+Arena−" task variant. Place avoidance of a 60° zone was reinforced by a constant
463 current foot shock (60 Hz, 500ms, 0.2mA) that was scrambled (5-poles) across pairs of the floor
464 rods. Rotation of the arena would carry the mouse into the shock zone unless the animal actively
465 avoided the zone. Entering the shock zone for more than 500 ms triggered shock. Additional
466 shocks occurred every 1.5 seconds until the animal left the shock zone. Measures of place
467 avoidance were computed by TrackAnalysis software (Bio-Signal Group Corp., Brooklyn, NY).
468 On day 1, mice received a 30-min trial with the shock off to habituate to the rotating arena.
469 Across the next two days the animals experienced 4 training trials, with 2 30-minute trials a day
470 with the activated shock with a 40 min inter-trial-interval.. Control (untrained mice) experienced
471 identical training conditions, except for the shock always being off.
472 Memory performance was assessed 24 hr after the final training session in a 10 minute retention
473 test with the shock off.
474
475 **Microdissected bulk RNA sequencing**
476 60 minutes after retention test, mice were euthanized and brains were extracted, washed in ice
477 washed in ice cold artificial cerebrospinal fluid, blocked, and mounted on a vibratome stage.
478 Hippocampal subregions (DG, CA3, CA1) were microdissected from 400 µm thick coronal live
479 tissue sections. Subregions from the dorsal hippocampus were extracted and microdissected
480 using microsurgical tools. Microdissected pieces of tissue from each animal were pooled by
481 subregion in 500 µL of prechilled TRIzol in a 1.5mL microcentrifuge tubes and stored at -80ºC.
482 Total RNA was extracted using the Zymo RNA mini prep kit (Zymo Research, Irvine, CA,
483 United States) according to the manufacturer's protocol. RNA quality was assessed on an

484 Agilent 2200 TapeStation (Agilent Technologies, Palo Alto, CA, United States). Samples with a
485 RIN greater than 7 were processed for library preparation. For library preparation NEBnext
486 ULTRA II RNA Library Preparation Kit for Illumina (New England Biolabs, Ipswich, MA,
487 United States) was used to: enrich mRNA from total RNA through rRNA depletion, fragment
488 mRNA into short fragments using fragmentation buffer, reverse transcribe mRNA into cDNA
489 using random primers, synthesize second-strand cDNA with DNA polymerase I, RNase H,
490 dNTP, and buffer. Double stranded cDNA fragments were preapered into sequenceable libraries
491 through multiple steps of purification using SPRIselect beads, end repair, A-tailing and adaptor
492 ligation. The ligated library was size selected using SPRIselect beads, PCR amplified and
493 sequenced using the Illumina Novaseq6000.
494
495 **Spatial transcriptomics**
496 60 minutes after retention test, mice were euthanized and brains were extracted and immediately
497 prepared for snap freezing in cuvettes of Tissue-Tek Optimal Cutting Temperature compound
498 (Sakura Finetek USA, Torrance, CA, United States) floating in a bath of methyl-butane chilled
499 by liquid nitrogen. Brain blocks were cryosectioned at -20ºC [114] and 10 µm thick coronal
500 sections containing the dorsal portion of the hippocampus were obtained (bregma -1.7 and -2.2
501 mm [115]). Collected tissue sections are trimmed to fit within the 5 mm x 5 mm capture area on
502 the Visium gene expression slide. Sections were mounted on a prechilled Visium gene
503 expression slide or a Tissue Optimization slide. A single tissue block was use to collect all tissue
504 sections mounted on the tissue optimization slide. One section of tissue per sample was mounted
505 in the capture areas of the Visium gene expression slide.

506 Tissue sections were fixed in chilled methanol and stained according to the Visium Spatial Gene
507 Expression User Guide [116] or Visium Spatial Tissue Optimization User Guide [117].
508 Tissues were permeabilized on the gene expression slide for 18 minutes which was selected from
509 the results of our tissue optimization experiment. Images were taken according to the Visium
510 Spatial Gene Expression Imaging Guidelines[118]. Brightfield histology images for the Visium
511 Tissue Optimization and Gene Expression slides were taken using the Leica Aperio CS2 Slide
512 Scanner at 20x magnification. Tissue optimization fluorescent images were taken on a Zeiss
513 LSM 800 (555nm LED,75% intensity, and 200ms exposure).
514 Tissue mRNA was extracted and libraries were prepared following the Visium Spatial Gene
515 Expression User Guide [116]. They were loaded at 300 pM and sequenced on a NovaSeq 6000
516 System (Illumina) using a NovaSeq S4 Reagent Kit (200 cycles, catalog no. 20027466,
517 Illumina), at a sequencing depth of approximately 250–400 10 × 106 read-pairs per sample.
518 Sequencing was performed using the following read protocol: read 1: 28 cycles; i7 index read:
519 10 cycles; i5 index read: 10 cycles; and read 2: 91 cycles.
520
521 **RNA sequencing data analysis**
522 Sequencing reads are processed at the Downstate Human Genomics Advanced Computing
523 Facility. Sequencing fastq files were demultiplexed with salmon, filtered and mapped to the
524 mouse MM10 reference genome [119] using STAR Aligner [120] and transcript reads were
525 quantified for each sample.
526
527 **Bulk RNA sequencing analyses**
528 *Differential Gene Expression*

529 Differential expression analysis was performed through DESeq2 on RNA counts between trained
530 and untrained sample groups. Genes with an of FDR below 0.05 were considered differentially
531 expressed genes/transcripts.

532 *PCA*

533 We ran 4 PCA analyses on normalized counts for samples. One analysis on all the the subregions
534 combined and 1 one the samples from each hippocampal subregion, 3 total.

535 *Heatmap*

536 Genewise Z-scores were calculated for the counts of each gene in each sample. Z-scores are
537 plotted as a heat map, where each row is a gene, and each column is a sample. Rows and
538 columns are then sorted in a dendrogram using Euclidean distance as a measurement for
539 similarity between any two given columns or rows.

540 *Gene Ontology Enrichment Analysis*

541 We used clusterProfiler's Overrepresentation analysis for GO terms [121] which uses the
542 hypergeometric test to calculate the enrichment Biological Processes, Cellular Components and
543 Molecular Functions amongst a list of differentially expressed genes (FDR < 0.05) against a
544 background of all detected genes. GO terms enriched with an FDR < 0.01 were considered
545 significant for our analyses. This analysis was also used for DEGs detected in the spatial
546 transcriptomic analyses. Dot plot figures show the top 10 GO terms ordered by significance for
547 each analysis plotted in the figured.

548 *Venn Diagram*

549 Vennplex software[122]was utilized to plot overlaps in the differentially expressed gene lists
550 from our regional differential gene expression analyses in a venn diagram format. This software,
551 stratifies gene lists by up- and down-regulated genes to display how many genes in overlapping

552 sectors are upregulated, downregulated or counterregulated (same gene with opposite effect sizes
553 in two regions).

554 *Gene overlap statistics*

555 The R-language package "SuperExactTest" [123] was used to statistically test the overlap of
556 gene names between regional lists of DEGs. The package uses the hypergeometric Fisher's Exact
557 test, against a background of all genes successfully compared in each differential gene
558 expression analysis. The software package also outputs an upset-style plot to visualize degree of
559 overlap between lists of DEGs and the level of significance of the overlap.

560

561 **Spatial transcriptomics analyses**

562 Reads from each sample were quantified and alighted to a predetermined loci or capture spots on
563 the histological image of each sample using 10x's space ranger software which references the
564 fiducial frame surrounding each capture area (10x Genomics Space Ranger 1.1.0).
565 Gene expression data were analyzed using the software package Seurat in the R coding
566 environment [124]. Spatial gene expression data were cropped to only include the capture spots
567 within the dorsal hippocampus. Data from each sample were then normalized, transformed and
568 integrated with one another using the default tools in Seurat. The integrated data set were further
569 normalized and clustered in PCA space. Clustered data can be visualized through UMAP
570 projections of the capture spots or in the 2D space of the tissue section. Cell type annotation was
571 performed by integrating our data with a random subset of 10,000 hippocampal cells from the
572 Allen Brain Atlas Cortex and Hippocampus Single Cell Taxonomy[56]. Predicted cell-type
573 identities were calculated and optimized based on gene expression similarity and anatomical
574 location.

575 *Differential Gene Expression*

576 Capture spots were grouped along two different criteria to calculate differential gene expression
577 in our samples. First, capture spots belonging to the anatomical cell layers of the Dentate Gyrus,
578 CA3 and CA1 regions were compared across training conditions together (All Regions) and
579 separately (region-wise). Next, within each training condition, hippocampal capture spots were
580 separated into two groups based on the detectable (>0) expression of the immediate early gene
581 (e.g. *Arc+* and *Arc-* groups). IEG expressing and not expressing groups of spots were compared
582 both within training conditions and across training conditions. Differential gene expression was
583 calculated using the Wilcoxon rank sum test (the default method for Seurat). Genes with an of
584 FDR below 0.05 were considered differentially expressed genes/transcripts.

585 *Pairwise Correlations*

586 Counts data for 23 known IEGs were extracted from hippocampal cell layer capture spots. In
587 each sample, Pearson's correlation coefficients were calculated pairwise for each IEG using the
588 base statistics in R-language. P values for Pearson's correlations were calculated for IEG's using
589 the base R-language correlation test.

590

591 **RT-qPCR**

592 Samples were extracted similarly to as described for bulk sample preparation to extract the dorsal
593 hippocampal subregions CA1,CA3, and DG from coronal sections of brain tissue. RNA
594 extraction using guanidinium-phenol-cholorform extraction with ethanol precipitation was
595 performed and quantified using spectrophotometry. cDNA was reverse transcribed from sample
596 bulk RNA using Thermo Fisher's SuperScript IV Kit (Thermo Fisher Scientific, Waltham, MA,
597 United States). Relative gene expression was quantified using the SYBR green master mix

598 system [125]. 10 µL reactions were prepared in the wells of a 384 well plate, hippocampal
599 regions were each prepared on separated plates. Each well contained 2.5ng of template cDNA
600 and 0.5 µM each of forward and reverse primers for one gene per well for a total reaction volume
601 of 10µL (sequences and melting temperatures can be found in table 1). Each gene was loaded in
602 triplicate in each plate to account for pipetting errors. Plates were incubated in the Bio-Rad
603 CFX384 Real-Time PCR Detection System (Bio-Rad Life Sciences, Hercules, CA, United
604 States) using the following schedule: 50°C for 5 min (1 cycle), 95°C for 10 min (1 cycle), 60°C
605 for 1 min (1 cycle), and 95°C for 15 s followed by 60°C for 1 min (40 cycles).

Gene	Direction	Sequence	Tm (°C)
Gahpdh	F	AGG TCG GTG TGA ACG GAT TG	57.47
	R	TGT AGA CCA TGT AGT TGA GTC A	52.84
Sst	F	ACC GGG AAA CAG GAA CTG G	57.44
	R	TTG CTG GGT TCG AGT TGG C	58.45
Kit	F	GCC ACG TCT CAG CCA TCT G	58.51
	R	GTC GCC AGC TTC AAC TAT TAA CT	55.14
Cdh24	F	AGC CTG TCC TTA TTG GCA AGC	57.92
	R	TGG GCC AGC AGC ACA TAT TG	58.33
Slc6a7	F	ACC TGG ATG TAG ACT TCG CAG	56.47
	R	CGC CAG ACA TTT CCC AAG C	56.97

Table 1. RT-qPCR primer sequences

Following 40 cycles of amplification wells were heated in a gradient from 55oC to 90oC to build dissociation curves of primers and their transcripts to assess primer efficiency and specificity. Ct values for each reaction are then automatically determined (roughly 20% of the plateau value). Data were analyzed for relative gene expression quantification using the ΔΔCt method, using the expression of *Gapdh* as the internal control. Relative expression values were normalized to the expression value of the untrained group and Student's t-test were performed on each primer target across training conditions using the ΔCt value for each comparison. Benjamini-Hochberg correction was performed to adjust p-values for multiple hypothesis testing.

617 **FIGURES**

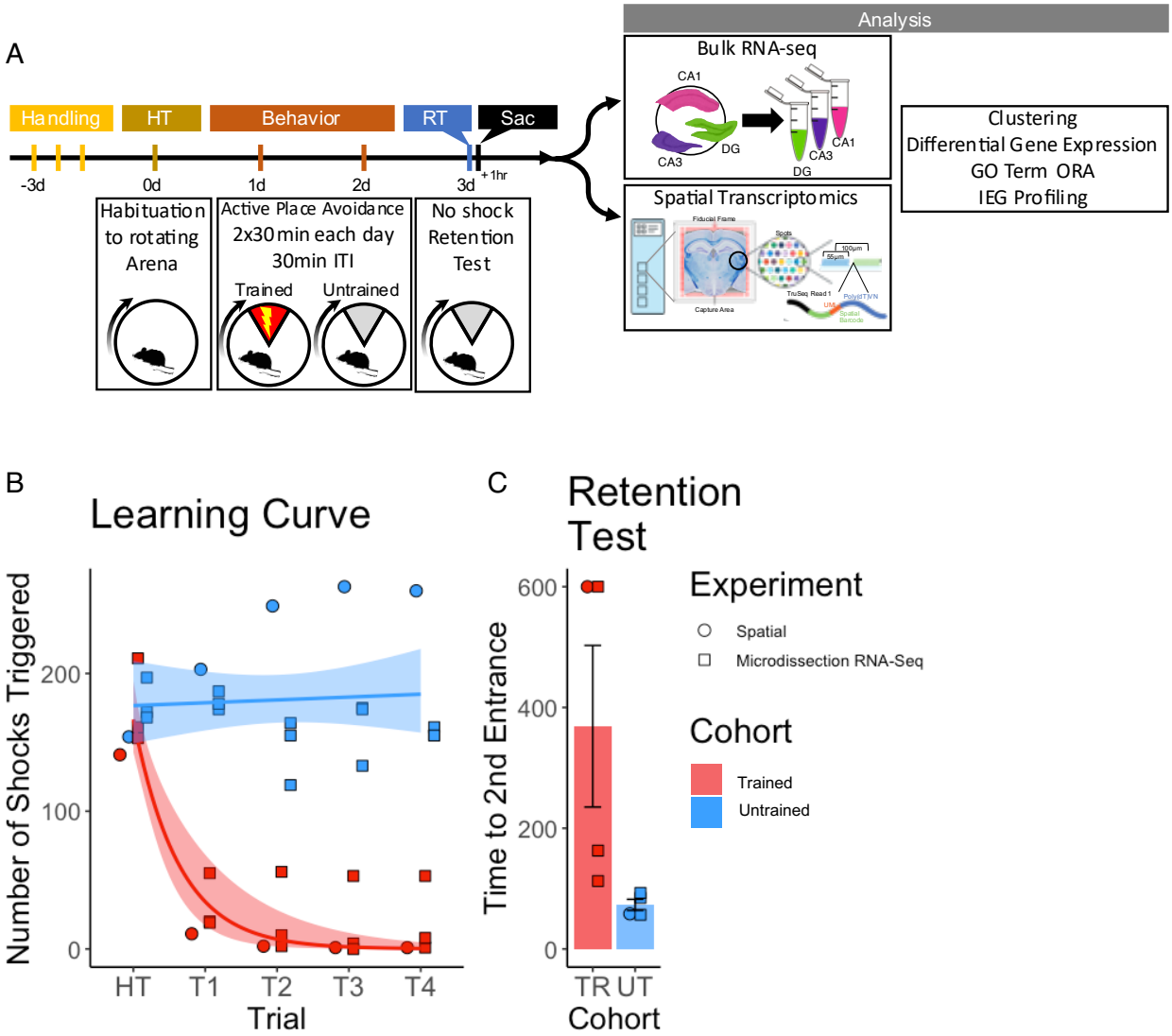

618

619 Figure 1. Trained mice learned to avoid the location of an unmarked shock zone

620 A) Experimental timeline. Mice were trained in the active place avoidance paradigm over the

621 course of 4 days following 3 days of handling. On day 0 they were habituated to a rotating arena

622 with no active shock zone (HT). On day 1 and 2 trained mice received two 30-minute trials with

623 an active shock zone. Untrained mice were not exposed to an active shock zone. On day 3 all

624 mice received a 10-minute retention test trial (exposed to the rotating arena with no active shock

625 zone). Mice were sacrificed 60 minutes following the end of the retention test, brains were
626 collected for further processing.
627 B) Training performance measured as number of shocks triggered. Trained mice learned to avoid
628 the location of the shock zone indicated by the decreased number of shocked triggered.
629 Exponential fit learning curves included with shaded error bars (SE).
630 C) Memory performance measured as time to second entrance in the retention test trial. Trained
631 mice showed higher time to second entrance during the retention test. Trained mean 375s ± 70.4
632 (SE), Untrained mean 58.7s ± 8.51 (SE).

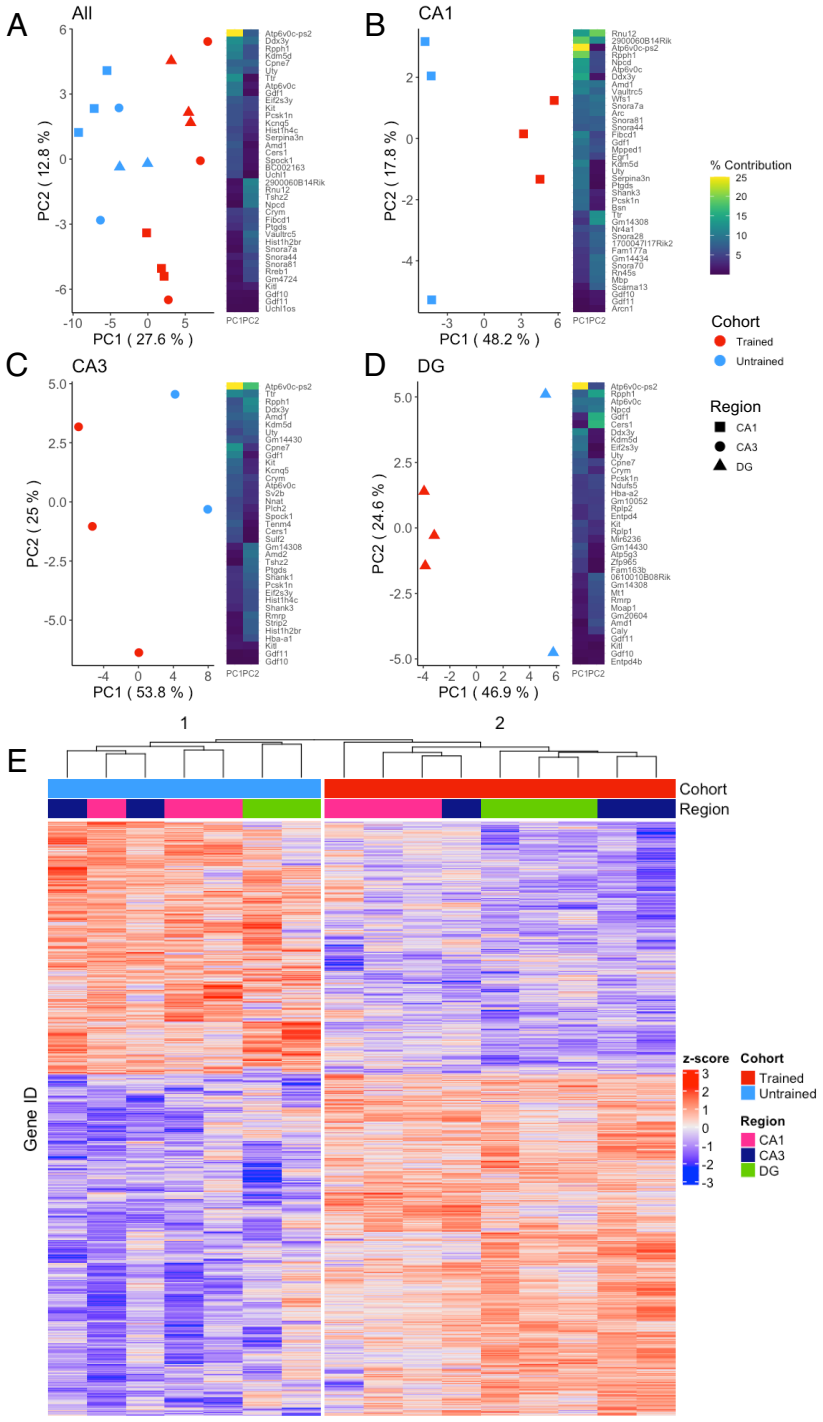

633

634 Figure 2. APA training results in substantial changes in hippocampal subregion gene expression

635 profiles

636 A-D) Left, principal component analyses of all hippocampal subregions (A), CA1 (B), CA3 (C),

637 DG (D) illustrate a clear separation between trained and untrained samples along the axis that

638 explains the most variance. Right, heatmap with top 20 contributing genes to the first two
639 principal components of each are reported in the heat map to the right of each plot. Sample size
640 for the CA1 was 3 trained and 3 untrained (B). Sample size for the CA3 was 3 trained and 2
641 untrained (C). And Sample size for the DG was 3 trained and 2 untrained (D).
642 E) Normalized gene expression of the top 2000 most significant DEGs. Hierarchical clustering of
643 gene expression profiles groups samples by behavioral cohort.

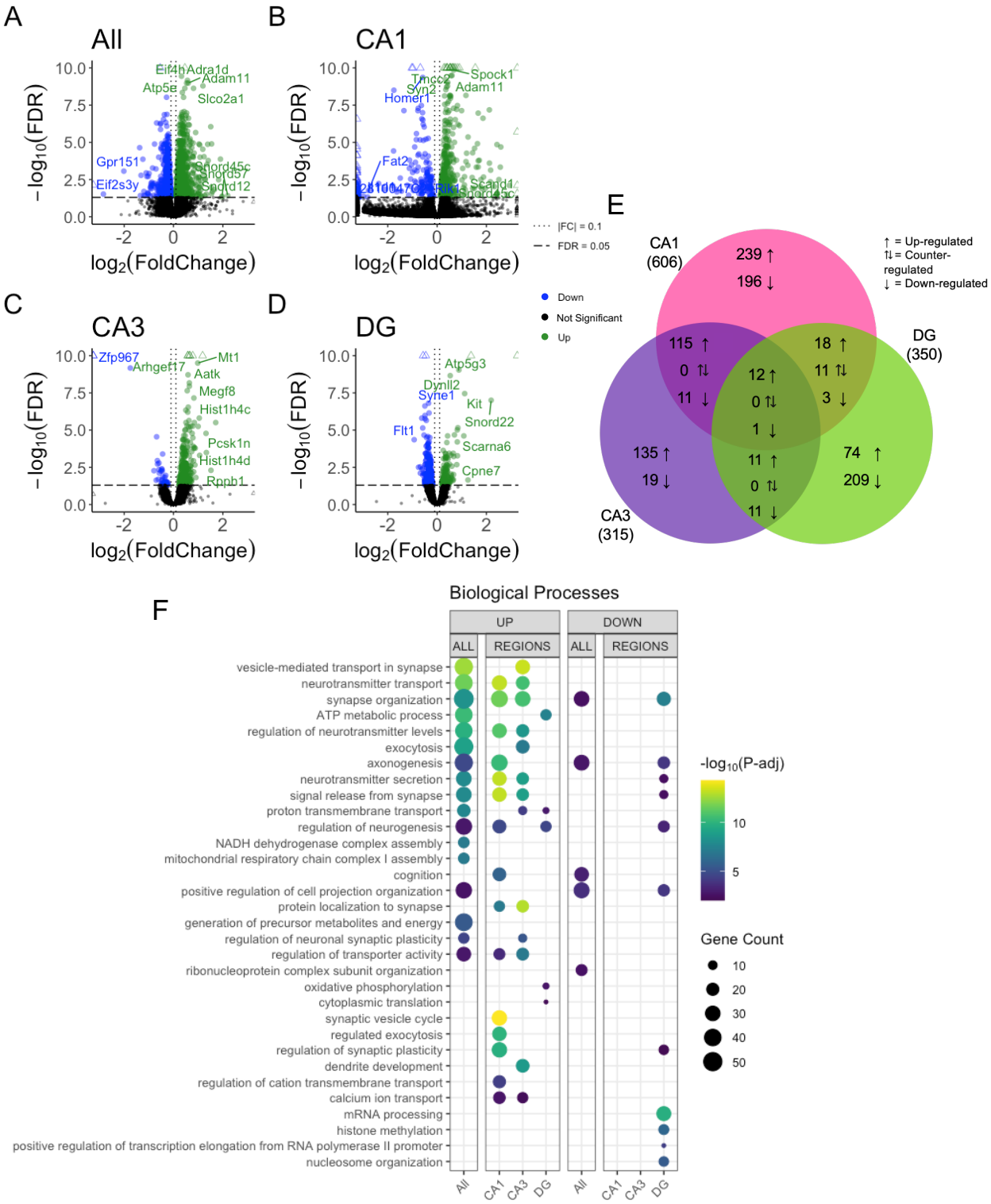
A
All
B
CA1
C
CA3
D
DG
E
F
Biological Processes
UP
DOWN
ALL
REGIONS
vesicle-mediated transport in synapse
neurotransmitter transport
synapse organization
ATP metabolic process
regulation of neurotransmitter levels
exocytosis
axonogenesis
neurotransmitter secretion
signal release from synapse
proton transmembrane transport
regulation of neurogenesis
NADH dehydrogenase complex assembly
mitochondrial respiratory chain complex I assembly
cognition
positive regulation of cell projection organization
protein localization to synapse
generation of precursor metabolites and energy
regulation of neuronal synaptic plasticity
regulation of transporter activity
ribonucleoprotein complex subunit organization
oxidative phosphorylation
cytoplasmic translation
synaptic vesicle cycle
regulated exocytosis
regulation of synaptic plasticity
dendrite development
regulation of cation transmembrane transport
calcium ion transport
mRNA processing
histone methylation
positive regulation of transcription elongation from RNA polymerase II promoter
nucleosome organization
All
CA1
CA3
DG
-log10(P-adj)
Gene Count
CA1 (606)
DG (350)
CA3 (315)
239 ↑
196 ↓
115 ↑
0 ⇅
11 ↓
18 ↑
11 ⇅
3 ↓
12 ↑
0 ⇅
1 ↓
135 ↑
19 ↓
74 ↑
209 ↓
11 ↑
0 ⇅
11 ↓
↑ = Up-regulated
⇅ = Counter-regulated
↓ = Down-regulated
|FC| = 0.1
FDR = 0.05
Down
Not Significant
Up

644

645 Figure 3. Bulk RNA-seq of hippocampal subregions reveals similar expression profiles in CA1
646 and CA3 regions in trained samples
647 A-D) Volcano plot of DEGs between trained and untrained in the CA1, CA3 and DG samples,
648 combined and individually. See Supplemental Figure 1A-D for full sized plots. E) Overlaps in
649 regional DEGs demonstrate greatest similarity between CA1 and CA3 subregions. DEGs from
650 each regional analysis were stratified by direction of fold change. Overlaps in DEGs between the
651 CA3 and CA1 subregions were significant (Fisher's Exact Test). See Supplemental Figure 1E for
652 further details. F) Biological processes overrepresented amongst DEGs detected between
653 samples from trained and untrained animals for CA1, CA3 and DG subregions (all combined and
654 separated). Dot color reflects the statistical significance ($-\log_{10}$(FDR)) of the biological process
655 enrichment. Dot size reflects the number of detected DEGs mapped to the genes involved in a
656 given biological process. See Supplemental Figure 1 for enrichment of Cellular Component and
657 Molecular Function GO terms.

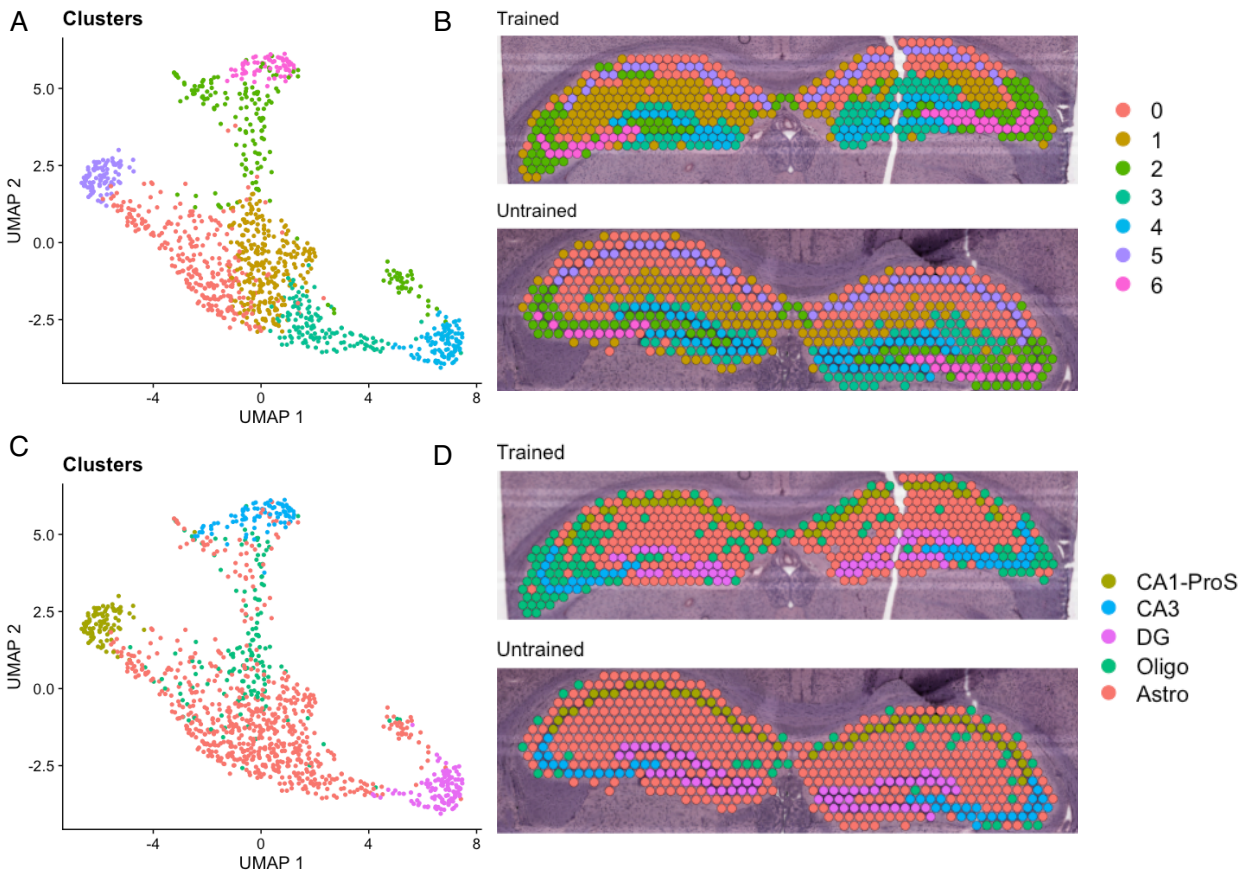

Figure 4. Clustering and cell-type annotation reflect anatomical boundaries of the hippocampal subregions

A,B) UMAP plot (left) and spatial transcriptomic maps of hippocampal spots (right) from trained and untrained mouse samples. Color reflects clustering of hippocampal spots. C,D) UMAP plot (left) and cell-type annotated spatial transcriptomic maps of hippocampal spots (right) in samples from the trained and untrained mouse.

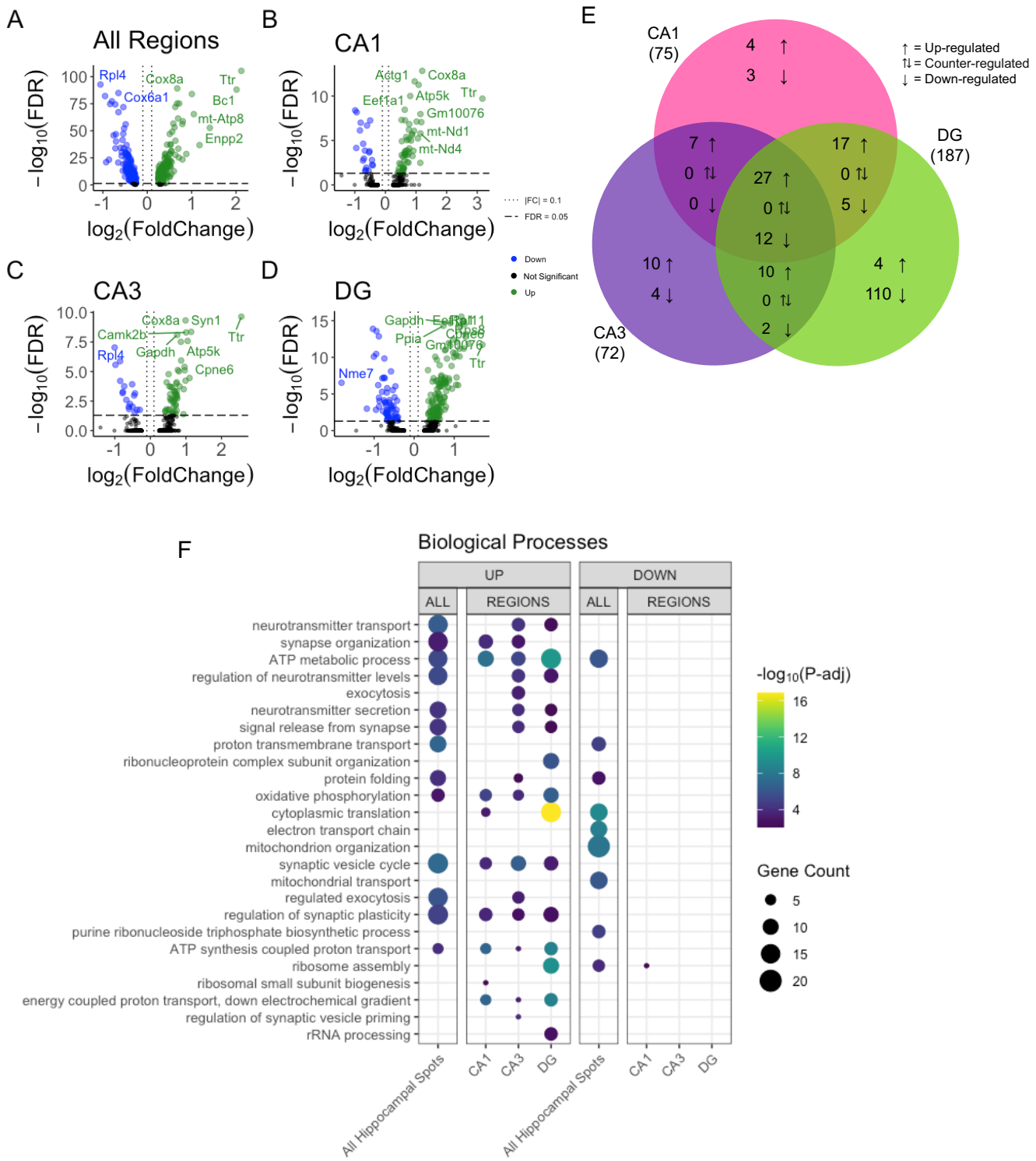
A
All Regions
B
CA1
C
CA3
D
DG
E
F
Biological Processes
UP
DOWN
ALL
REGIONS
neurotransmitter transport
synapse organization
ATP metabolic process
regulation of neurotransmitter levels
exocytosis
neurotransmitter secretion
signal release from synapse
proton transmembrane transport
ribonucleoprotein complex subunit organization
protein folding
oxidative phosphorylation
cytoplasmic translation
electron transport chain
mitochondrion organization
synaptic vesicle cycle
mitochondrial transport
regulated exocytosis
regulation of synaptic plasticity
purine ribonucleoside triphosphate biosynthetic process
ATP synthesis coupled proton transport
ribosome assembly
ribosomal small subunit biogenesis
energy coupled proton transport, down electrochemical gradient
regulation of synaptic vesicle priming
rRNA processing
All Hippocampal Spots
CA1
CA3
DG
-log10(P-adj)
Gene Count
CA1 (75)
DG (187)
CA3 (72)
↑ = Up-regulated
⇅ = Counter-regulated
↓ = Down-regulated

665

666 Figure 5. DEGs detected between trained and untrained animals within hippocampal subregions
667 using spatial transcriptomics are enriched with genes involved in similar biological processes to
668 those seen in bulk RNA-seq
669 A-D) Volcano plot of DEGs between all hippocampal (A), CA1 (B), CA3 (C), and DG (D) cell-
670 layer spots from trained and untrained mice. E) Overlap of regionally detected DEGs stratified
671 by direction of fold change. Overlaps were tested with Fisher's exact test. See Supplemental
672 Figure 2A for further details. F) Biological processes overrepresented amongst DEGs detected
673 between samples from trained and untrained animals for hippocampal samples or all
674 hippocampal spots, and spots from the separated CA1, CA3 and DG cell layers. Dot color
675 reflects the statistical significance ($-\log_{10}$(FDR)) of the biological process enrichment. Dot size
676 reflects the number of detected DEGs mapped to the genes involved in a given biological
677 process. See Supplemental Figure 2 for enrichment of Cellular Component and Molecular
678 Function GO terms.

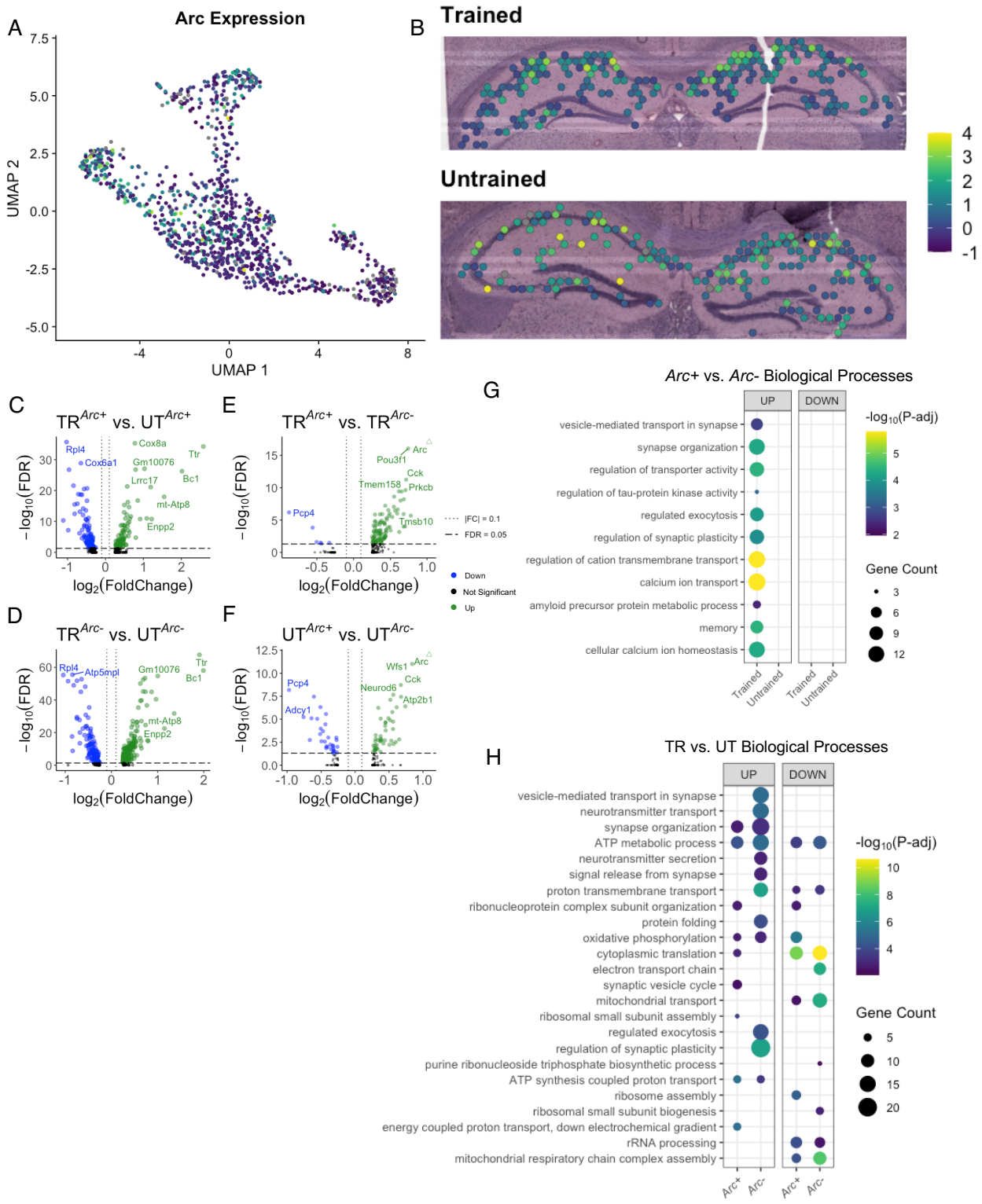
A
Arc Expression
UMAP 2
UMAP 1
B
Trained
Untrained
C
TR^Arc+ vs. UT^Arc+
D
TR^Arc- vs. UT^Arc-
E
TR^Arc+ vs. TR^Arc-
F
UT^Arc+ vs. UT^Arc-
log2(FoldChange)
-log10(FDR)
|FC| = 0.1
FDR = 0.05
Down
Not Significant
Up
G
Arc+ vs. Arc- Biological Processes
UP
DOWN
vesicle-mediated transport in synapse
synapse organization
regulation of transporter activity
regulation of tau-protein kinase activity
regulated exocytosis
regulation of synaptic plasticity
regulation of cation transmembrane transport
calcium ion transport
amyloid precursor protein metabolic process
memory
cellular calcium ion homeostasis
Trained
Untrained
-log10(P-adj)
Gene Count
H
TR vs. UT Biological Processes
vesicle-mediated transport in synapse
neurotransmitter transport
synapse organization
ATP metabolic process
neurotransmitter secretion
signal release from synapse
proton transmembrane transport
ribonucleoprotein complex subunit organization
protein folding
oxidative phosphorylation
cytoplasmic translation
electron transport chain
synaptic vesicle cycle
mitochondrial transport
ribosomal small subunit assembly
regulated exocytosis
regulation of synaptic plasticity
purine ribonucleoside triphosphate biosynthetic process
ATP synthesis coupled proton transport
ribosome assembly
ribosomal small subunit biogenesis
energy coupled proton transport, down electrochemical gradient
rRNA processing
mitochondrial respiratory chain complex assembly
Arc+
Arc-
-log10(P-adj)
Gene Count

679

680 Figure 6. Arc-positive spots in the trained sample are enriched with genes involved in synaptic
681 plasticity
682 A,B) UMAP plot (left) and spatial transcriptomic maps of hippocampal spots (right) in the
683 trained and untrained samples. Colors show normalized expression of the *Arc* gene in
684 hippocampal cell layer spots. C,D) Volcano plots of differential gene expression of *Arc* positive
685 (C) and negative (D) spots across behavioral conditions. E,F) Volcano plots of differential gene
686 expression between *Arc* positive and negative spots within trained (E) and untrained (F) samples.
687 G) Biological processes overrepresented amongst DEGs detected in the analysis of *Arc*-
688 expressing spots within trained and untrained samples. Dot color reflects the statistical
689 significance ($-\log_{10}$(FDR)) of the biological process enrichment. Dot size reflects the number of
690 detected DEGs mapped to the genes involved in a given biological process. H) Biological
691 processes overrepresented amongst DEGs detected in the analysis of *Arc*-expressing spots across
692 trained and untrained samples. Dot color reflects the statistical significance ($-\log_{10}$(FDR)) of the
693 biological process enrichment. Dot size reflects the number of detected DEGs mapped to the
694 genes involved in a given biological process.

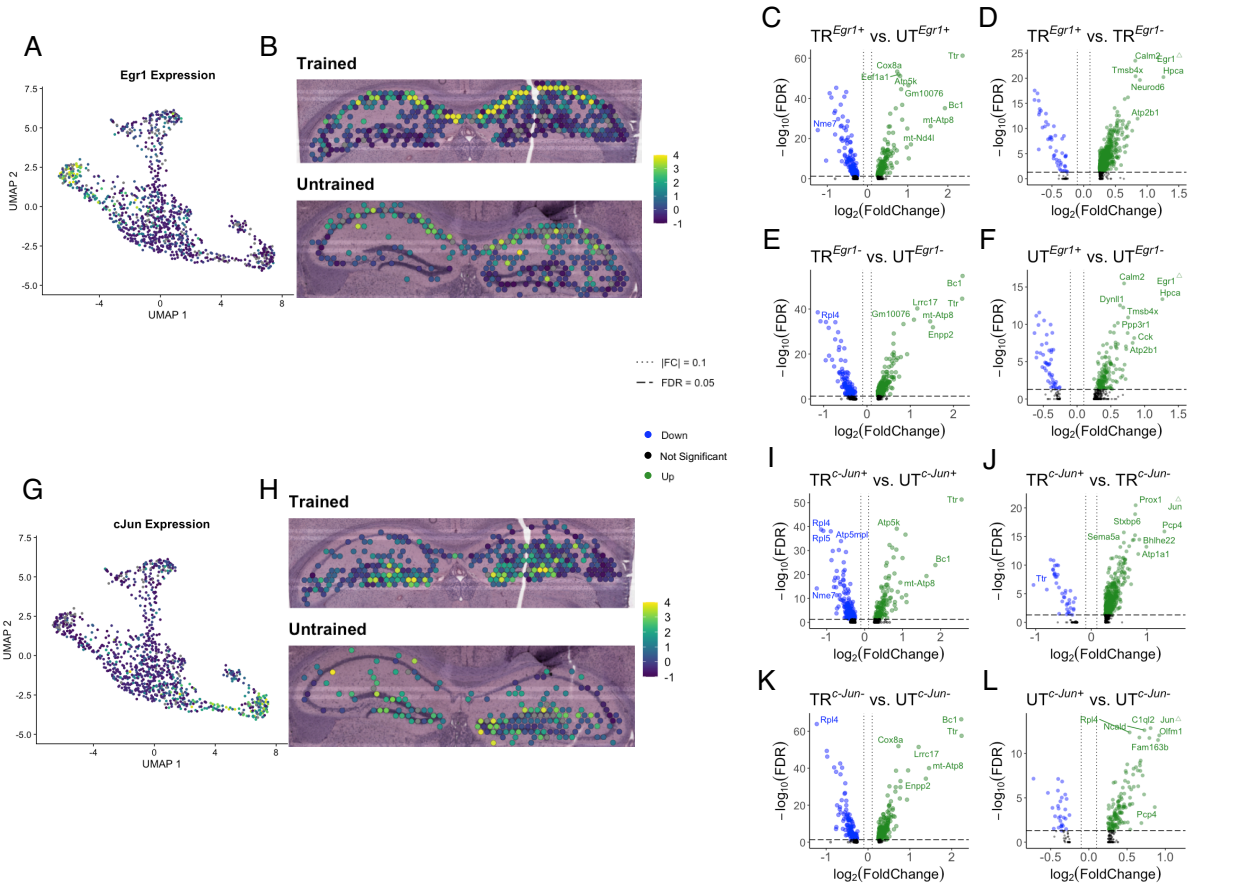
A
Egr1 Expression
UMAP 2
UMAP 1
B
Trained
Untrained
|FC| = 0.1
FDR = 0.05
Down
Not Significant
Up
C
TR^Egr1+ vs. UT^Egr1+
D
TR^Egr1+ vs. TR^Egr1-
E
TR^Egr1- vs. UT^Egr1-
F
UT^Egr1+ vs. UT^Egr1-
G
cJun Expression
H
Trained
Untrained
I
TR^c-Jun+ vs. UT^c-Jun+
J
TR^c-Jun+ vs. TR^c-Jun-
K
TR^c-Jun- vs. UT^c-Jun-
L
UT^c-Jun+ vs. UT^c-Jun-
−log10(FDR)
log2(FoldChange)

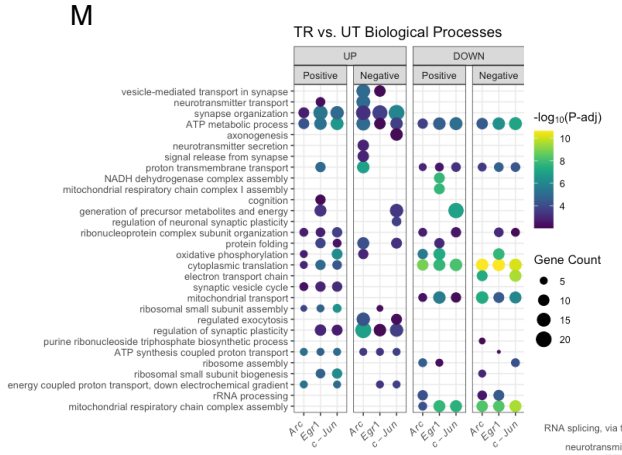
M
TR vs. UT Biological Processes
UP
DOWN
Positive
Negative
vesicle-mediated transport in synapse
neurotransmitter transport
synapse organization
ATP metabolic process
axonogenesis
neurotransmitter secretion
signal release from synapse
proton transmembrane transport
NADH dehydrogenase complex assembly
mitochondrial respiratory chain complex I assembly
cognition
generation of precursor metabolites and energy
regulation of neuronal synaptic plasticity
ribonucleoprotein complex subunit organization
protein folding
oxidative phosphorylation
cytoplasmic translation
electron transport chain
synaptic vesicle cycle
mitochondrial transport
ribosomal small subunit assembly
regulated exocytosis
regulation of synaptic plasticity
purine ribonucleoside triphosphate biosynthetic process
ATP synthesis coupled proton transport
ribosome assembly
ribosomal small subunit biogenesis
energy coupled proton transport, down electrochemical gradient
rRNA processing
mitochondrial respiratory chain complex assembly
Arc
Egr1
c-Jun
-log10(P-adj)
Gene Count

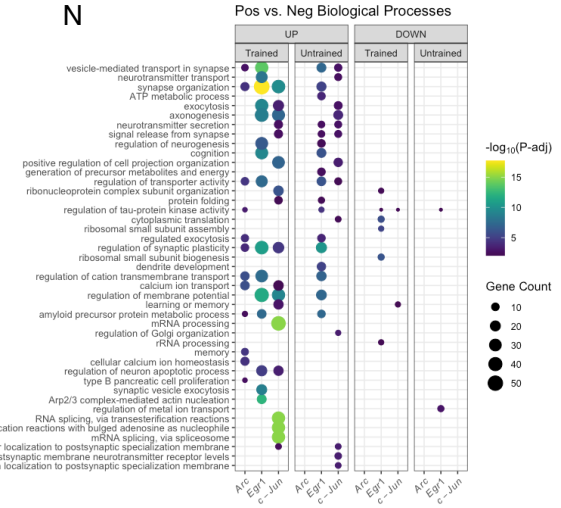
N
Pos vs. Neg Biological Processes
UP
DOWN
Trained
Untrained
vesicle-mediated transport in synapse
neurotransmitter transport
synapse organization
ATP metabolic process
exocytosis
axonogenesis
neurotransmitter secretion
signal release from synapse
regulation of neurogenesis
cognition
positive regulation of cell projection organization
generation of precursor metabolites and energy
regulation of transporter activity
ribonucleoprotein complex subunit organization
protein folding
regulation of tau-protein kinase activity
cytoplasmic translation
ribosomal small subunit assembly
regulated exocytosis
regulation of synaptic plasticity
ribosomal small subunit biogenesis
dendrite development
regulation of cation transmembrane transport
calcium ion transport
regulation of membrane potential
learning or memory
amyloid precursor protein metabolic process
mRNA processing
regulation of Golgi organization
rRNA processing
memory
cellular calcium ion homeostasis
regulation of neuron apoptotic process
type B pancreatic cell proliferation
synaptic vesicle exocytosis
Arp2/3 complex-mediated actin nucleation
regulation of metal ion transport
RNA splicing, via transesterification reactions
RNA splicing, via transesterification reactions with bulged adenosine as nucleophile
mRNA splicing, via spliceosome
neurotransmitter receptor localization to postsynaptic specialization membrane
regulation of postsynaptic membrane neurotransmitter receptor levels
protein localization to postsynaptic specialization membrane
Arc
Egr1
c-Jun
-log10(P-adj)
Gene Count

695

696 Figure 7. Spatial transcriptomics reveals distinct collections of biological processes enriched
697 among *Arc*, *Egr1*, and *c-Jun*-expressing spots
698 A,B) UMAP plot (left) and spatial transcriptomic maps (right) of hippocampal spots in the
699 trained and untrained sample. Color reflects the normalized expression of Egr1 in the
700 hippocampal cell layer spots. C,D,E,F) Volcano plots of differential gene expression of Egr1
701 positive (C) and negative (D) spots across behavioral conditions and within trained (E) and
702 untrained (F) samples. G,H) UMAP plot (left) and spatial transcriptomic maps (right) of
703 hippocampal spots in the trained and untrained samples. Color reflects normalized expression of
704 c-Jun in the hippocampal cell layer spots. I,J,K,L) Volcano plots of differential gene expression
705 of c-Jun positive (I) and negative (K) spots across behavioral conditions and within trained (J)
706 and untrained (L) samples. M) Biological processes overrepresented amongst DEGs in Arc,
707 Egr1, and c-Jun-expressing spots between trained and untrained samples. Dot color reflects
708 statistical significance (-log10(FDR)) of biological process enrichment. Dot size reflects number
709 of detected DEGs mapped to the genes involved in a given biological process. N) Biological
710 processes overrepresented amongst DEGs in Arc, Egr1, and c-Jun-expressing spots across
711 trained and untrained samples. Dot color reflects statistical significance (-log10(FDR)) of
712 biological process enrichment. Dot size reflects the number of detected DEGs mapped to the
713 genes involved in a given biological process.

714 **SUPPLEMENTAL FIGURES**

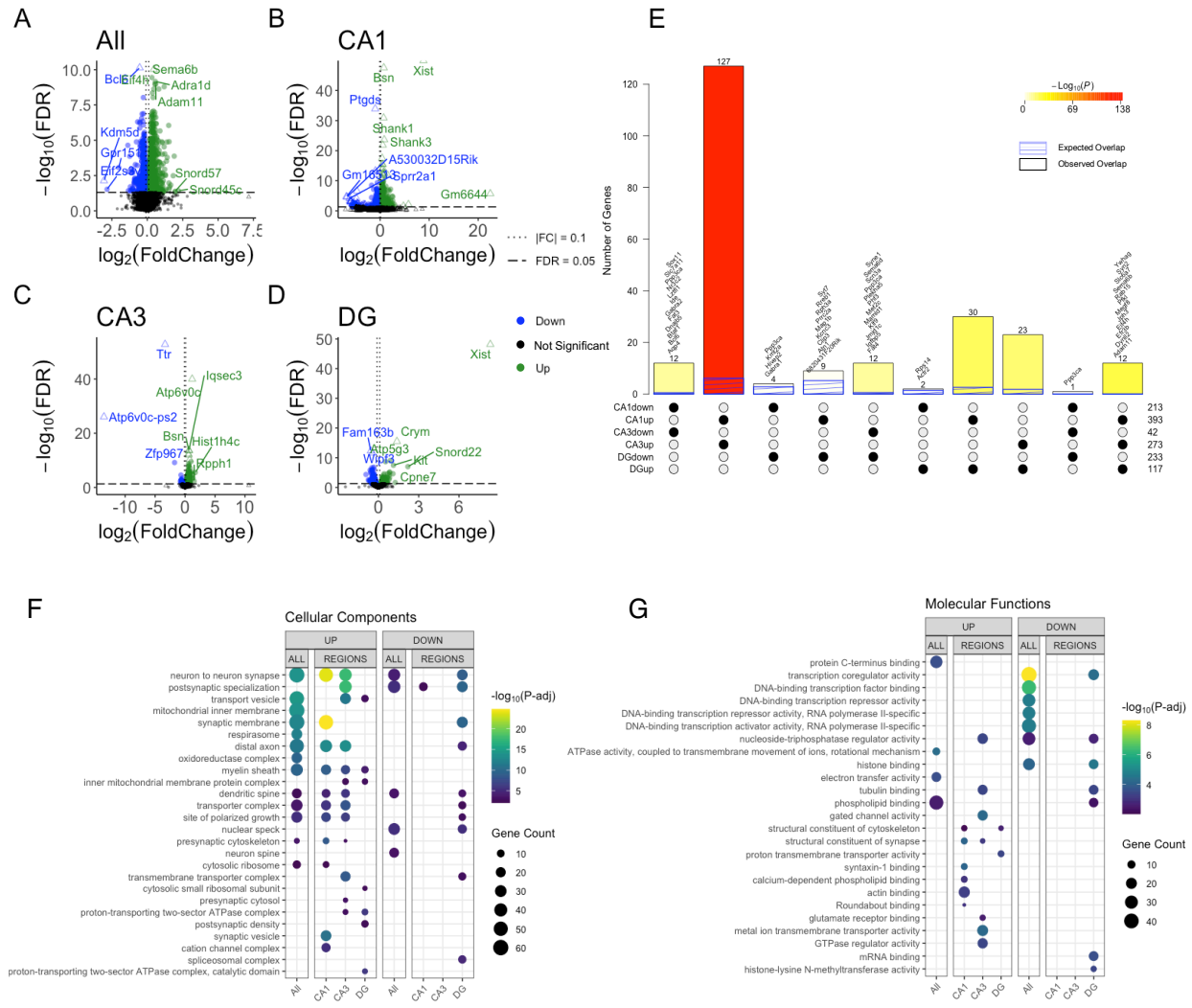

715

716 Supplemental Figure 1. Trained CA1 and CA3 subregions express similar DEGs and

717 postsynaptic cellular component GO terms

718 A-D) Volcano plot of DEGs between trained and untrained CA1, CA3 and DG samples,

719 combined and individually. Triangular points mark data out of the frame of the main text figure.

720 E) Upset plot of overlaps in regional DEGs demonstrates greatest similarity between CA1 and

721 CA3 samples. DEGs from each regional analysis were stratified by direction of fold change. In

722 the upset plot, each bar represents the number of genes in an intersection of lists of DEGs. The

723 intersecting lists is represented by the dots underneath the bar. The hashed line on each bar

724 represents the expected intersection of two identically sized random lists. Overlaps were tested
725 with Fisher's exact test using the list of all expressed genes as a background. The color of the
726 bar represents the $-\log_{10}(P)$ for the BH corrected P-value of each intersection. F,G) Cellular
727 compartments (F) and molecular functions (G)overrepresented amongst DEGs detected between
728 the hippocampal subregions from trained and untrained samples for all regions combined and
729 separated CA1, CA3 and DG samples. Dot color reflects the statistical significance (-
730 $\log_{10}(FDR)$) of the biological process enrichment. Dot size reflects the number of detected DEGs
731 mapped to the genes involved in a given biological process.

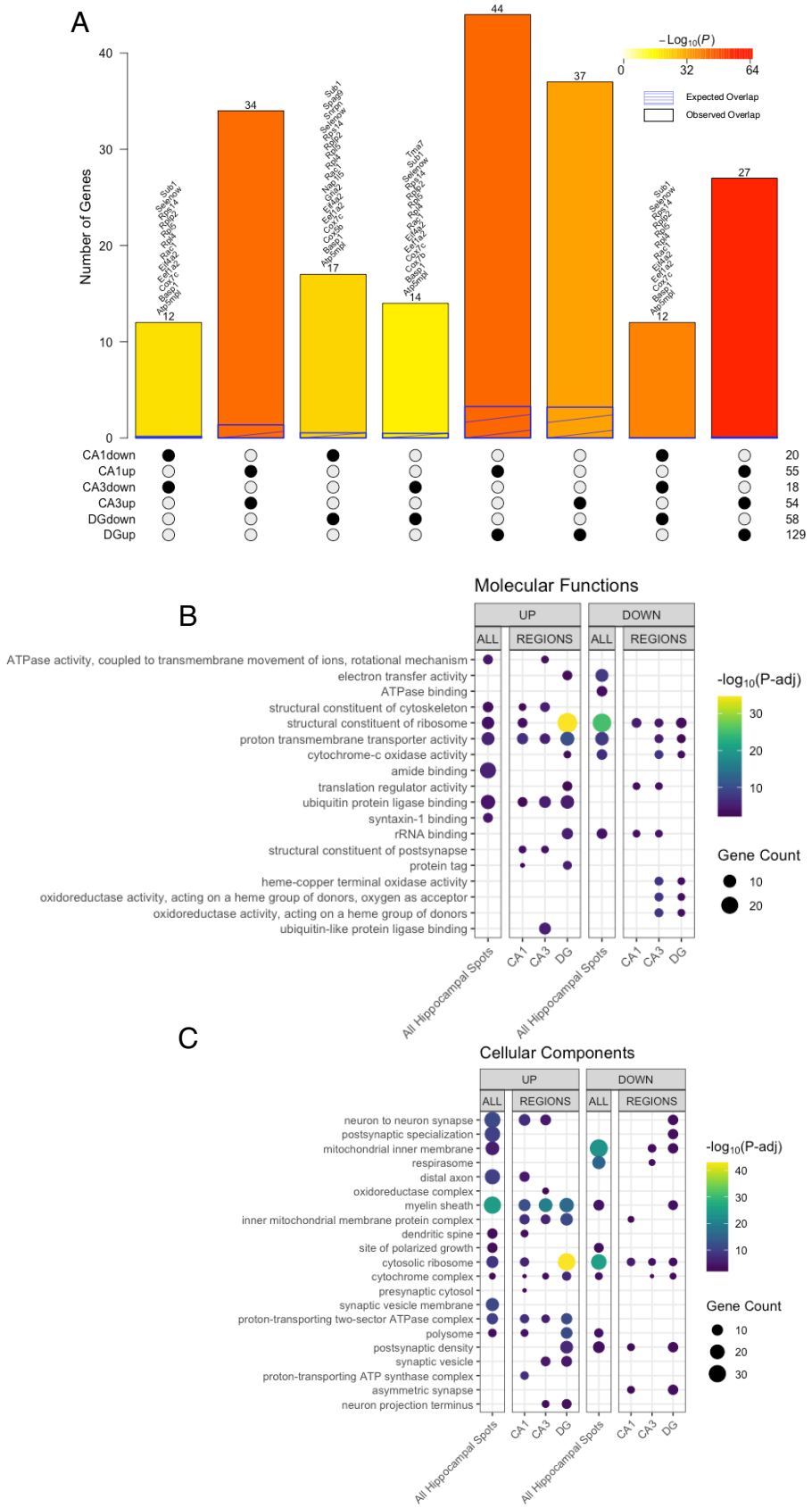
A
Number of Genes
−Log10(P)
0
32
64
Expected Overlap
Observed Overlap
CA1down
CA1up
CA3down
CA3up
DGdown
DGup
12
34
17
14
44
37
12
27
20
55
18
54
58
129
B
Molecular Functions
UP
DOWN
ALL
REGIONS
ATPase activity, coupled to transmembrane movement of ions, rotational mechanism
electron transfer activity
ATPase binding
structural constituent of cytoskeleton
structural constituent of ribosome
proton transmembrane transporter activity
cytochrome-c oxidase activity
amide binding
translation regulator activity
ubiquitin protein ligase binding
syntaxin-1 binding
rRNA binding
structural constituent of postsynapse
protein tag
heme-copper terminal oxidase activity
oxidoreductase activity, acting on a heme group of donors, oxygen as acceptor
oxidoreductase activity, acting on a heme group of donors
ubiquitin-like protein ligase binding
All Hippocampal Spots
CA1
CA3
DG
-log10(P-adj)
Gene Count
C
Cellular Components
neuron to neuron synapse
postsynaptic specialization
mitochondrial inner membrane
respirasome
distal axon
oxidoreductase complex
myelin sheath
inner mitochondrial membrane protein complex
dendritic spine
site of polarized growth
cytosolic ribosome
cytochrome complex
presynaptic cytosol
synaptic vesicle membrane
proton-transporting two-sector ATPase complex
polysome
postsynaptic density
synaptic vesicle
proton-transporting ATP synthase complex
asymmetric synapse
neuron projection terminus

732

733 Supplemental Figure 2. Cellular components and molecular functions enriched among DEGs
734 detected using spatial transcriptomics
735 A) Upset plot of overlaps in regional DEGs demonstrates greatest similarity between CA1 and
736 CA3 subregions. DEGs from each regional analysis were stratified by direction of fold change.
737 In the upset plot, each bar represents the number of genes in an intersection of lists of DEGs. The
738 intersecting lists is represented by the dots underneath the bar. The hashed line on each bar
739 represents the expected intersection of two identically sized random lists. Overlaps were tested
740 with Fisher's exact test using the list of all expressed genes as a background. The color of the
741 bar represents the $-\log_{10}(P)$ for the BH corrected P-value of each intersection. B,C) Molecular
742 functions (B) and cellular compartments (C) overrepresented amongst DEGs detected between
743 the hippocampal samples from trained and untrained samples for all hippocampal spots and spots
744 in the cell layers of CA1, CA3 and DG subregions. Dot color reflects the statistical significance
745 ($-\log_{10}(FDR)$) of the biological process enrichment. Dot size reflects the number of detected
746 DEGs mapped to the genes involved in a given biological process.

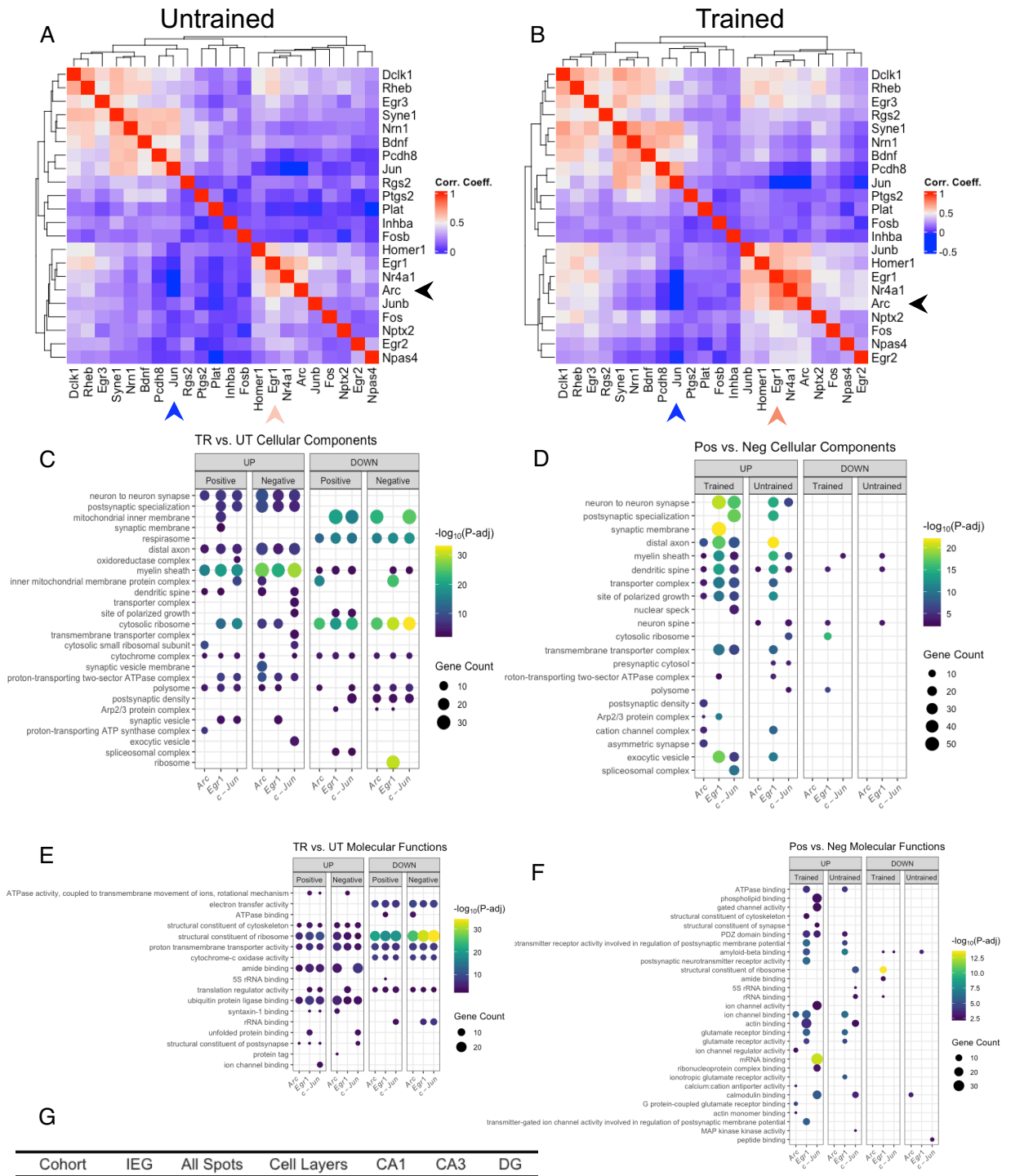

G

Cohort	IEG	All Spots	Cell Layers	CA1	CA3	DG
Trained	Arc	195/542	56/146	34/49	20/43	2/54
	Egr1	380/542	130/146	48/49	41/43	41/54
	c-Jun	308/542	106/146	22/49	32/43	52/54
Untrained	Arc	169/568	58/155	34/51	19/42	5/62
	Egr1	256/568	113/155	51/51	33/42	29/62
	c-Jun	175/568	83/155	12/51	18/42	53/62

747

748 Supplemental Figure 3. The expression of the IEGs *Egr1* and *c-Jun* are most and least correlated
749 with the expression of *Arc*, respectively
750 A, B) Heatmaps reflecting the pairwise Pearson correlation coefficients between IEGs detected
751 in the Trained (A) and Untrained (B) sample. Pearson correlation between *Arc* and *Egr1* or *c-Jun*
752 are marked by the caret on the x-axis colored to reflect the value of the correlation coefficient.
753 The correlation coefficients for *Arc* and *Egr1* are $r(21) = .598$, $p = 2.24 \times 10^{-56}$ in the untrained
754 sample and $r(21) = .764$, $p = 5.45 \times 10^{-105}$ in the trained sample. The correlation coefficients for
755 *Arc* and *c-Jun* are $r(21) = -.057$, $p = 0.17$ in the untrained sample and $r(21) = -.105$, $p = 0.014$ in
756 the trained sample. C,E) Molecular functions (C) and cellular compartments (E) overrepresented
757 amongst DEGs detected across trained and untrained samples for spots expressionr the IEGs *Arc*,
758 *Egr1*, and *c-Jun*. Dot color reflects the statistical significance ($-\log_{10}$(FDR)) of the biological
759 process enrichment. Dot size reflects the number of detected DEGs mapping to the gene
760 belonging to a given biological process D,F) Molecular functions (D) and cellular compartments
761 (F) overrepresented amongst DEGs detected between IEG positive and negative spots within
762 either the trained or untrained sample. Dot color reflects the statistical significance ($-\log_{10}$(FDR))
763 of the biological process enrichment. Dot size reflects the number of detected DEGs mapping to
764 the gene belonging to a given biological process G) Table total number of IEG expressing spots
765 relative to the total number of hippocampal spots for each area.

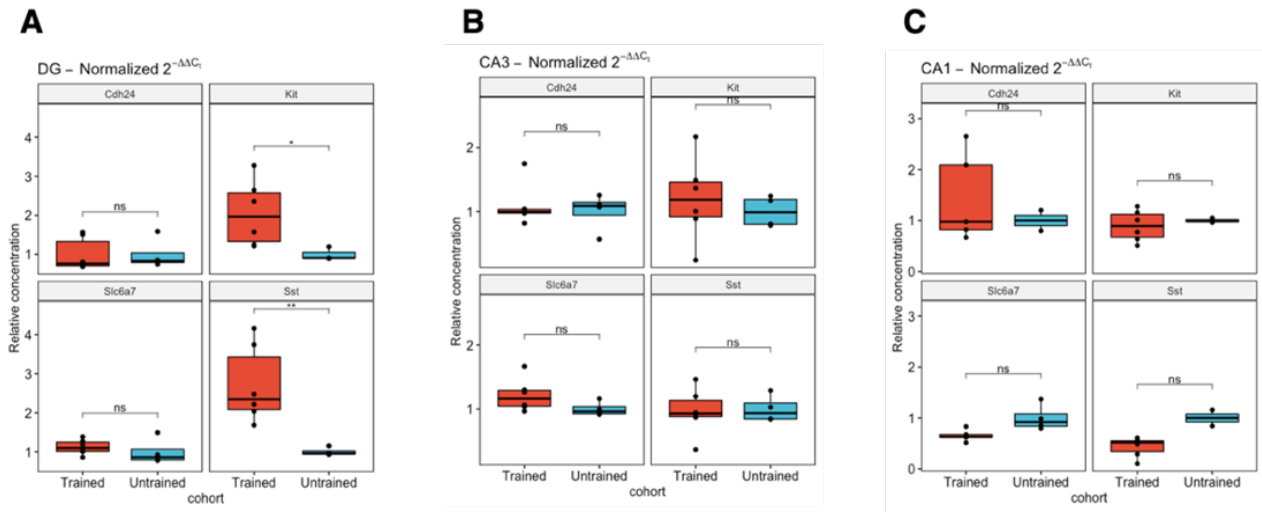

Supplemental Figure 4. Relative expression of select DEGs through RT-qPCR

A-C)Average normalized relative expression ($2^{-\Delta\Delta Ct}$) of genes in trained samples (red) as compared to untrained samples (blue) in dentate gyrus (A), CA3 (B) and CA1 (C) subregions. n= 6 trained and n=4 untrained animals. Student t-test was performed between ΔCt values from trained and untrained samples for each gene.

REFERENCES

1. Kitamura, T., et al., *Engrams and circuits crucial for systems consolidation of a memory.* Science, 2017. **356**(6333): p. 73-78.
2. Josselyn, S.A. and S. Tonegawa, *Memory engrams: Recalling the past and imagining the future.* Science, 2020. **367**(6473).
3. Takeuchi, T., A.J. Duszkiewicz, and R.G. Morris, *The synaptic plasticity and memory hypothesis: encoding, storage and persistence.* Philos Trans R Soc Lond B Biol Sci, 2014. **369**(1633): p. 20130288.
4. Malenka, R.C. and M.F. Bear, *LTP and LTD: an embarrassment of riches.* Neuron, 2004. **44**(1): p. 5-21.
5. Mayford, M., S.A. Siegelbaum, and E.R. Kandel, *Synapses and memory storage.* Cold Spring Harb Perspect Biol, 2012. **4**(6).
6. Marco, A., et al., *Mapping the epigenomic and transcriptomic interplay during memory formation and recall in the hippocampal engram ensemble.* Nat Neurosci, 2020. **23**(12): p. 1606-1617.
7. Rao-Ruiz, P., et al., *Engram-specific transcriptome profiling of contextual memory consolidation.* Nat Commun, 2019. **10**(1): p. 2232.
8. Reshetnikov, V.V., et al., *Genes associated with cognitive performance in the Morris water maze: an RNA-seq study.* Sci Rep, 2020. **10**(1): p. 22078.
9. Poo, M.M., et al., *What is memory? The present state of the engram.* BMC Biol, 2016. **14**: p. 40.
10. Mayford, M., *The search for a hippocampal engram.* Philos Trans R Soc Lond B Biol Sci, 2014. **369**(1633): p. 20130161.
11. Middleton, S.J. and T.J. McHugh, *CA2: A Highly Connected Intrahippocampal Relay.* Annu Rev Neurosci, 2020. **43**: p. 55-72.
12. Chevaleyre, V. and S.A. Siegelbaum, *Strong CA2 pyramidal neuron synapses define a powerful disynaptic cortico-hippocampal loop.* Neuron, 2010. **66**(4): p. 560-572.
13. Senzai, Y., *Function of local circuits in the hippocampal dentate gyrus-CA3 system.* Neurosci Res, 2019. **140**: p. 43-52.
14. Basu, J. and S.A. Siegelbaum, *The Corticohippocampal Circuit, Synaptic Plasticity, and Memory.* Cold Spring Harb Perspect Biol, 2015. **7**(11).
15. Amaral, D.G. and M.P. Witter, *The three-dimensional organization of the hippocampal formation: a review of anatomical data.* Neuroscience, 1989. **31**(3): p. 571-91.
16. Sloviter, R.S. and T. Lomo, *Updating the lamellar hypothesis of hippocampal organization.* Front Neural Circuits, 2012. **6**: p. 102.
17. van Strien, N.M., N.L. Cappaert, and M.P. Witter, *The anatomy of memory: an interactive overview of the parahippocampal-hippocampal network.* Nat Rev Neurosci, 2009. **10**(4): p. 272-82.
18. Kesner, R.P., I. Lee, and P. Gilbert, *A behavioral assessment of hippocampal function based on a subregional analysis.* Rev Neurosci, 2004. **15**(5): p. 333-51.
19. Lisman, J.E., *Relating hippocampal circuitry to function: recall of memory sequences by reciprocal dentate-CA3 interactions.* Neuron, 1999. **22**(2): p. 233-42.
20. Ryan, T.J., et al., *Memory. Engram cells retain memory under retrograde amnesia.* Science, 2015. **348**(6238): p. 1007-13.
21. Hunsaker, M.R. and R.P. Kesner, *The operation of pattern separation and pattern completion processes associated with different attributes or domains of memory.* Neurosci Biobehav Rev, 2013. **37**(1): p. 36-58.
22. Molitor, R.J., et al., *Memory Reactivation during Learning Simultaneously Promotes Dentate Gyrus/CA_{2,3} Pattern Differentiation and CA₁ Memory Integration.* The Journal of Neuroscience, 2021. **41**(4): p. 726-738.
23. Shpokayte, M., et al., *Hippocampal cells segregate positive and negative engrams.* Commun Biol, 2022. **5**(1): p. 1009.
24. Sullivan, K.E., R.M. Kendrick, and M.S. Cembrowski, *Elucidating memory in the brain via single-cell transcriptomics.* J Neurochem, 2021. **157**(4): p. 982-992.

25. Shah, S., et al., *In Situ Transcription Profiling of Single Cells Reveals Spatial Organization of Cells in the Mouse Hippocampus.* Neuron, 2016. **92**(2): p. 342-357.
26. Cho, J.H., B.S. Huang, and J.M. Gray, *RNA sequencing from neural ensembles activated during fear conditioning in the mouse temporal association cortex.* Sci Rep, 2016. **6**: p. 31753.
27. Tonegawa, S., M.D. Morrissey, and T. Kitamura, *The role of engram cells in the systems consolidation of memory.* Nat Rev Neurosci, 2018. **19**(8): p. 485-498.
28. Sanes, J.R. and J.W. Lichtman, *Can molecules explain long-term potentiation?* Nat Neurosci, 1999. **2**(7): p. 597-604.
29. Alberini, C.M. and E.R. Kandel, *The regulation of transcription in memory consolidation.* Cold Spring Harb Perspect Biol, 2014. **7**(1): p. a021741.
30. Asok, A., et al., *Molecular Mechanisms of the Memory Trace.* Trends Neurosci, 2019. **42**(1): p. 14-22.
31. Magee, J.C. and C. Grienberger, *Synaptic Plasticity Forms and Functions.* Annual Review of Neuroscience, 2020. **43**(1): p. 95-117.
32. Guan, J.S., et al., *How Does the Sparse Memory "Engram" Neurons Encode the Memory of a Spatial-Temporal Event?* Front Neural Circuits, 2016. **10**: p. 61.
33. Chen, B.K., et al., *Artificially Enhancing and Suppressing Hippocampus-Mediated Memories.* Curr Biol, 2019. **29**(11): p. 1885-1894 e4.
34. Sauvage, M., T. Kitsukawa, and E. Atucha, *Single-cell memory trace imaging with immediate-early genes.* J Neurosci Methods, 2019. **326**: p. 108368.
35. Meenakshi, P., S. Kumar, and J. Balaji, *In vivo imaging of immediate early gene expression dynamics segregates neuronal ensemble of memories of dual events.* Mol Brain, 2021. **14**(1): p. 102.
36. Erwin, S.R., et al., *A Sparse, Spatially Biased Subtype of Mature Granule Cell Dominates Recruitment in Hippocampal-Associated Behaviors.* Cell Rep, 2020. **31**(4): p. 107551.
37. Guzowski, J.F., et al., *Environment-specific expression of the immediate-early gene Arc in hippocampal neuronal ensembles.* Nat Neurosci, 1999. **2**(12): p. 1120-4.
38. Ramirez-Amaya, V., et al., *Spatial exploration-induced Arc mRNA and protein expression: evidence for selective, network-specific reactivation.* J Neurosci, 2005. **25**(7): p. 1761-8.
39. Lee, B.H., et al., *Real-time visualization of mRNA synthesis during memory formation in live mice.* Proc Natl Acad Sci U S A, 2022. **119**(27): p. e2117076119.
40. Cimadevilla, J.M., et al., *Passive and active place avoidance as a tool of spatial memory research in rats.* J Neurosci Methods, 2000. **102**(2): p. 155-64.
41. Stuchlík, A., et al., *Place Avoidance Tasks as Tools in the Behavioral Neuroscience of Learning and Memory.* Physiological Research, 2013: p. S1-S19.
42. Wachi, T., B. Cornell, and K. Toyo-Oka, *Complete ablation of the 14-3-3epsilon protein results in multiple defects in neuropsychiatric behaviors.* Behav Brain Res, 2017. **319**: p. 31-36.
43. Annamneedi, A., et al., *The Presynaptic Scaffold Protein Bassoon in Forebrain Excitatory Neurons Mediates Hippocampal Circuit Maturation: Potential Involvement of TrkB Signalling.* Int J Mol Sci, 2021. **22**(15).
44. Leone, L., et al., *Altered Nup153 Expression Impairs the Function of Cultured Hippocampal Neural Stem Cells Isolated from a Mouse Model of Alzheimer's Disease.* Mol Neurobiol, 2019. **56**(8): p. 5934-5949.
45. Vigil, F.A., et al., *Prevention of long-term memory loss after retrieval by an endogenous CaMKII inhibitor.* Sci Rep, 2017. **7**(1): p. 4040.
46. Urrutia-Ruiz, C., et al., *Deletion of the Autism-Associated Protein SHANK3 Abolishes Structural Synaptic Plasticity after Brain Trauma.* Int J Mol Sci, 2022. **23**(11).
47. Hung, A.Y., et al., *Smaller dendritic spines, weaker synaptic transmission, but enhanced spatial learning in mice lacking Shank1.* J Neurosci, 2008. **28**(7): p. 1697-708.
48. Hou, Q., et al., *SNAP-25 in hippocampal CA1 region is involved in memory consolidation.* Eur J Neurosci, 2004. **20**(6): p. 1593-603.

49. Gomis-Gonzalez, M., et al., *Protein Kinase C-Gamma Knockout Mice Show Impaired Hippocampal Short-Term Memory While Preserved Long-Term Memory.* Mol Neurobiol, 2021. **58**(2): p. 617-630.
50. Iqbal, J., *Transthyretin—A Key Gene Involved in Regulating Learning and Memory in Brain, and Providing Neuroprotection in Alzheimer Disease via Neuronal Synthesis of Transthyretin Protein.* Scientific Research Publishing, 2018. **8**(2).
51. Pratt, K.J.B., et al., *Loss of neuronal Tet2 enhances hippocampal-dependent cognitive function.* Cell Rep, 2022. **41**(6): p. 111612.
52. Katafuchi, T., et al., *Impairment of spatial learning and hippocampal synaptic potentiation in c-kit mutant rats.* Learn Mem, 2000. **7**(6): p. 383-92.
53. Ferreira, E., D.M. Shaw, and S. Oddo, *Identification of learning-induced changes in protein networks in the hippocampi of a mouse model of Alzheimer's disease.* Transl Psychiatry, 2016. **6**(7): p. e849.
54. Barbieri, R., et al., *Synapsin I and Synapsin II regulate neurogenesis in the dentate gyrus of adult mice.* Oncotarget, 2018. **9**(27): p. 18760-18774.
55. The Gene Ontology, C., *The Gene Ontology Resource: 20 years and still GOing strong.* Nucleic Acids Res, 2019. **47**(D1): p. D330-D338.
56. Yao, Z., et al., *A taxonomy of transcriptomic cell types across the isocortex and hippocampal formation.* Cell, 2021. **184**(12): p. 3222-3241 e26.
57. Schober, D.A., et al., *Transmembrane AMPA receptor regulatory proteins and cornichon-2 allosterically regulate AMPA receptor antagonists and potentiators.* J Biol Chem, 2011. **286**(15): p. 13134-42.
58. Lugara, E., et al., *Synapsin I Controls Synaptic Maturation of Long-Range Projections in the Lateral Amygdala in a Targeted Selective Fashion.* Front Cell Neurosci, 2019. **13**: p. 220.
59. Nicole, O. and E. Pacary, *CaMKIIbeta in Neuronal Development and Plasticity: An Emerging Candidate in Brain Diseases.* Int J Mol Sci, 2020. **21**(19).
60. Carrillo-Reid, L., *Neuronal ensembles in memory processes.* Semin Cell Dev Biol, 2022. **125**: p. 136-143.
61. Gouty-Colomer, L.A., et al., *Arc expression identifies the lateral amygdala fear memory trace.* Mol Psychiatry, 2016. **21**(3): p. 364-75.
62. Hsieh, C., et al., *Persistent increases of PKMzeta in memory-activated neurons trace LTP maintenance during spatial long-term memory storage.* Eur J Neurosci, 2021. **54**(8): p. 6795-6814.
63. Chia, C. and T. Otto, *Hippocampal Arc (Arg3.1) expression is induced by memory recall and required for memory reconsolidation in trace fear conditioning.* Neurobiol Learn Mem, 2013. **106**: p. 48-55.
64. Zhang, T., et al., *Expression of BC1 Impairs Spatial Learning and Memory in Alzheimer's Disease Via APP Translation.* Mol Neurobiol, 2018. **55**(7): p. 6007-6020.
65. Liu, Y., et al., *Hippocampal Activation of Rac1 Regulates the Forgetting of Object Recognition Memory.* Curr Biol, 2016. **26**(17): p. 2351-7.
66. Zhang, L., et al., *Dickkopf 3 (Dkk3) Improves Amyloid-beta Pathology, Cognitive Dysfunction, and Cerebral Glucose Metabolism in a Transgenic Mouse Model of Alzheimer's Disease.* J Alzheimers Dis, 2017. **60**(2): p. 733-746.
67. Hadjiivanova, C., S. Belcheva, and I. Belcheva, *Cholecystokinin and learning and memory processes.* Acta Physiol Pharmacol Bulg, 2003. **27**(2-3): p. 83-8.
68. Tutukova, S., V. Tarabykin, and L.R. Hernandez-Miranda, *The Role of Neurod Genes in Brain Development, Function, and Disease.* Front Mol Neurosci, 2021. **14**: p. 662774.
69. Sun, X., et al., *Functionally Distinct Neuronal Ensembles within the Memory Engram.* Cell, 2020. **181**(2): p. 410-423 e17.
70. Nambu, M.F., et al., *What does engram encode?: Heterogeneous memory engrams for different aspects of experience.* Curr Opin Neurobiol, 2022. **75**: p. 102568.

71. Okuno, H., *Regulation and function of immediate-early genes in the brain: beyond neuronal activity markers.* Neurosci Res, 2011. **69**(3): p. 175-86.
72. Gallo, F.T., et al., *Immediate Early Genes, Memory and Psychiatric Disorders: Focus on c-Fos, Egr1 and Arc.* Front Behav Neurosci, 2018. **12**: p. 79.
73. Vanrobaeys, Y., et al., *Mapping the spatial transcriptomic signature of the hippocampus during memory consolidation.* Nat Commun, 2023. **14**(1): p. 6100.
74. Rolls, E.T., *Memory systems in the brain.* Annu Rev Psychol, 2000. **51**: p. 599-630.
75. Stanfield, B.B. and W.M. Cowan, *The morphology of the hippocampus and dentate gyrus in normal and reeler mice.* J Comp Neurol, 1979. **185**(3): p. 393-422.
76. Khalaf-Nazzal, R. and F. Francis, *Hippocampal development - old and new findings.* Neuroscience, 2013. **248**: p. 225-42.
77. Cembrowski, M.S. and N. Spruston, *Heterogeneity within classical cell types is the rule: lessons from hippocampal pyramidal neurons.* Nat Rev Neurosci, 2019. **20**(4): p. 193-204.
78. Montgomery, S.M. and G. Buzsaki, *Gamma oscillations dynamically couple hippocampal CA3 and CA1 regions during memory task performance.* Proc Natl Acad Sci U S A, 2007. **104**(36): p. 14495-500.
79. Carr, M.F., M.P. Karlsson, and L.M. Frank, *Transient slow gamma synchrony underlies hippocampal memory replay.* Neuron, 2012. **75**(4): p. 700-13.
80. Alam, M.J., et al., *Adult Neurogenesis Conserves Hippocampal Memory Capacity.* J Neurosci, 2018. **38**(31): p. 6854-6863.
81. Kitamura, T., et al., *Adult neurogenesis modulates the hippocampus-dependent period of associative fear memory.* Cell, 2009. **139**(4): p. 814-27.
82. Kitamura, T. and K. Inokuchi, *Role of adult neurogenesis in hippocampal-cortical memory consolidation.* Mol Brain, 2014. **7**: p. 13.
83. Deng, W., J.B. Aimone, and F.H. Gage, *New neurons and new memories: how does adult hippocampal neurogenesis affect learning and memory?* Nat Rev Neurosci, 2010. **11**(5): p. 339-50.
84. Aksoy-Aksel, A. and D. Manahan-Vaughan, *The temporoammonic input to the hippocampal CA1 region displays distinctly different synaptic plasticity compared to the Schaffer collateral input in vivo: significance for synaptic information processing.* Front Synaptic Neurosci, 2013. **5**: p. 5.
85. Pavlowsky, A. and J.M. Alarcon, *Interaction between long-term potentiation and depression in CA1 synapses: temporal constrains, functional compartmentalization and protein synthesis.* PLoS One, 2012. **7**(1): p. e29865.
86. Mendez-Lopez, M., et al., *Spatial short-term memory in rats: effects of learning trials on metabolic activity of limbic structures.* Neurosci Lett, 2010. **483**(1): p. 32-5.
87. Christie, S.T. and P. Schrater, *Cognitive cost as dynamic allocation of energetic resources.* Front Neurosci, 2015. **9**: p. 289.
88. Terranova, J.I., et al., *Hippocampal-amygdala memory circuits govern experience-dependent observational fear.* Neuron, 2022. **110**(8): p. 1416-1431 e13.
89. Roy, D.S., et al., *Distinct Neural Circuits for the Formation and Retrieval of Episodic Memories.* Cell, 2017. **170**(5): p. 1000-1012 e19.
90. Marks, W.D., et al., *Neuronal Ensembles Organize Activity to Generate Contextual Memory.* Front Behav Neurosci, 2022. **16**: p. 805132.
91. Li, X. and C.Y. Wang, *From bulk, single-cell to spatial RNA sequencing.* Int J Oral Sci, 2021. **13**(1): p. 36.
92. Stahl, P.L., et al., *Visualization and analysis of gene expression in tissue sections by spatial transcriptomics.* Science, 2016. **353**(6294): p. 78-82.
93. Asp, M., J. Bergenstrahle, and J. Lundeberg, *Spatially Resolved Transcriptomes-Next Generation Tools for Tissue Exploration.* Bioessays, 2020. **42**(10): p. e1900221.
94. Yap, E.L. and M.E. Greenberg, *Activity-Regulated Transcription: Bridging the Gap between Neural Activity and Behavior.* Neuron, 2018. **100**(2): p. 330-348.

95. Sheng, M. and M.E. Greenberg, *The regulation and function of c-fos and other immediate early genes in the nervous system.* Neuron, 1990. **4**(4): p. 477-85.
96. Jeong, Y., et al., *Synaptic plasticity-dependent competition rule influences memory formation.* Nat Commun, 2021. **12**(1): p. 3915.
97. Magistretti, P.J. and I. Allaman, *A cellular perspective on brain energy metabolism and functional imaging.* Neuron, 2015. **86**(4): p. 883-901.
98. Wesierska, M., C. Dockery, and A.A. Fenton, *Beyond memory, navigation, and inhibition: behavioral evidence for hippocampus-dependent cognitive coordination in the rat.* J Neurosci, 2005. **25**(9): p. 2413-9.
99. Lacagnina, A.F., et al., *Distinct hippocampal engrams control extinction and relapse of fear memory.* Nat Neurosci, 2019. **22**(5): p. 753-761.
100. Sweis, B.M., et al., *Dynamic and heterogeneous neural ensembles contribute to a memory engram.* Curr Opin Neurobiol, 2021. **67**: p. 199-206.
101. Tonegawa, S., et al., *Memory engram storage and retrieval.* Curr Opin Neurobiol, 2015. **35**: p. 101-9.
102. Terranova, J.I., et al., *Systems consolidation induces multiple memory engrams for a flexible recall strategy in observational fear memory in male mice.* Nat Commun, 2023. **14**(1): p. 3976.
103. Sun, X. and Y. Lin, *Npas4: Linking Neuronal Activity to Memory.* Trends Neurosci, 2016. **39**(4): p. 264-275.
104. Sheng, H.Z., R.D. Fields, and P.G. Nelson, *Specific regulation of immediate early genes by patterned neuronal activity.* J Neurosci Res, 1993. **35**(5): p. 459-67.
105. Guzowski, J.F., et al., *Experience-dependent gene expression in the rat hippocampus after spatial learning: a comparison of the immediate-early genes Arc, c-fos, and zif268.* J Neurosci, 2001. **21**(14): p. 5089-98.
106. Lyons, M.R. and A.E. West, *Mechanisms of specificity in neuronal activity-regulated gene transcription.* Prog Neurobiol, 2011. **94**(3): p. 259-95.
107. Madabhushi, R. and T.K. Kim, *Emerging themes in neuronal activity-dependent gene expression.* Mol Cell Neurosci, 2018. **87**: p. 27-34.
108. Tyssowski, K.M., et al., *Different Neuronal Activity Patterns Induce Different Gene Expression Programs.* Neuron, 2018. **98**(3): p. 530-546 e11.
109. Flavell, S.W. and M.E. Greenberg, *Signaling mechanisms linking neuronal activity to gene expression and plasticity of the nervous system.* Annu Rev Neurosci, 2008. **31**: p. 563-90.
110. Cheval, H., et al., *Distinctive features of Egr transcription factor regulation and DNA binding activity in CA1 of the hippocampus in synaptic plasticity and consolidation and reconsolidation of fear memory.* Hippocampus, 2012. **22**(3): p. 631-42.
111. Maddox, S.A., M.S. Monsey, and G.E. Schafe, *Early growth response gene 1 (Egr-1) is required for new and reactivated fear memories in the lateral amygdala.* Learn Mem, 2011. **18**(1): p. 24-38.
112. Sherrin, T., et al., *Hippocampal c-Jun-N-terminal kinases serve as negative regulators of associative learning.* J Neurosci, 2010. **30**(40): p. 13348-61.
113. Denny, C.A., et al., *Hippocampal memory traces are differentially modulated by experience, time, and adult neurogenesis.* Neuron, 2014. **83**(1): p. 189-201.
114. 10x Genomics, *Visium Spatial Protocols – Tissue Preparation Guide.* 2023.
115. Paxinos, G. and K.B.J. Franklin, *Paxinos and Franklin's the Mouse Brain in Stereotaxic Coordinates*. 2019: Elsevier Science.
116. Genomics, x., *Visium Spatial Gene Expression Reagent Kits User Guide.* 2023.
117. Genomics, x., *Visium Spatial Gene Expression Reagent Kits - Tissue Optimization.* 2019.
118. Genomics, x., *Visium Spatial Gene Expression Imaging Guidelines.* 2021.
119. Consortium, G.R., *Genome Reference Consortium Mouse Build 38*. 2012.
120. Dobin, A., et al., *STAR: ultrafast universal RNA-seq aligner.* Bioinformatics, 2013. **29**(1): p. 15-21.

1025 121. Wu, T., et al., *clusterProfiler 4.0: A universal enrichment tool for interpreting omics data.*
1026 Innovation (Camb), 2021. **2**(3): p. 100141.
1027 122. Cai, H., et al., *VennPlex–A Novel Venn Diagram Program for Comparing and Visualizing Datasets*
1028 *with Differentially Regulated Datapoints.* PLoS ONE, 2013. **8**(1): p. e53388.
1029 123. Wang, M., Y. Zhao, and B. Zhang, *Efficient Test and Visualization of Multi-Set Intersections.* Sci
1030 Rep, 2015. **5**: p. 16923.
1031 124. Butler, A., et al., *Integrating single-cell transcriptomic data across different conditions,*
1032 *technologies, and species.* Nat Biotechnol, 2018. **36**(5): p. 411-420.
1033 125. Ponchel, F., et al., *Real-time PCR based on SYBR-Green I fluorescence: an alternative to the*
1034 *TaqMan assay for a relative quantification of gene rearrangements, gene amplifications and micro*
1035 *gene deletions.* BMC Biotechnol, 2003. **3**: p. 18.
1036